A Polygonal Spline Method for General Second-Order Elliptic Equations and Its Applications

Ming-Jun Lai and James Lanterman

Abstract We explain how to use polygonal splines to numerically solve second-order elliptic partial differential equations. The convergence of the polygonal spline method will be studied. Also, we will use this approach to numerically study the solution of some mixed parabolic and hyperbolic partial differential equations. Comparison with standard bivariate spline method will be given to demonstrate that our polygonal splines have some better numerical performance.

Keywords Polygonal splines · Generalized barycentric coordinates · Numerical solution of PDEs

1 Introduction

Traditionally, people use triangulations to numerically solve partial differential equations (PDEs). A new trend is to use more general polygonal meshes. That is, we can be more versatile and efficient than the standard finite element method when numerically solving PDEs. See [2–4] for a so-called virtual element method to solve PDEs based on arbitrary polygonal meshes. In [17], the researchers use C^0 generalized barycentric coordinate (GBC) elements to solve the standard Poisson equations in 2D and 3D over arbitrary convex polygonal partitions. In [20], the researchers construct C^0 quadratic finite elements based on GBC to solve PDEs. In [18], these researchers use the weak Galerkin method based on rectangular partitions to solve second-order elliptic PDEs. In [12], the researchers constructed a class of continuous polygonal

This research is partially supported by Simons Collaboration Grant 280646 and the National Science Foundation under the Grant #DMS 1521537.

M.-J. Lai (✉) · J. Lanterman
Department of Mathematics, University of Georgia, Athens, GA 30602, USA
e-mail: mjlai@math.uga.edu

J. Lanterman
e-mail: jay@math.uga.edu

G.E. Fasshauer and L.L. Schumaker (eds.), *Approximation Theory XV: San Antonio 2016*, Springer Proceedings in Mathematics & Statistics 201,
DOI 10.1007/978-3-319-59912-0_6

finite elements of arbitrary order d which allows for reproduction of polynomials of total degree d. These elements were implemented for numerical solution of Poisson equations. In this paper, we shall explore how to use these polygonal elements to solve general second-order elliptic PDEs and some mixed parabolic and hyperbolic partial differential equations.

A model PDE problem considered in this paper can be described as follows. Let Ω be a bounded open polyhedral domain in $\mathbb{R}^2$, and let $\Gamma = \partial\Omega$ be the boundary of Ω. We consider the following general second-order PDE:

$$\begin{cases} \mathscr{L}(u) = f, & \mathbf{x} \in \Omega \\ u = g, & \mathbf{x} \in \Gamma \end{cases} \tag{1}$$

where $\mathbf{x} = (x_1, x_2) \in \mathbb{R}^2$ and $\mathscr{L}$ is a partial differential operator in the following form:

$$\mathscr{L}(u) := -\sum_{i,j=1}^{2} \frac{\partial}{\partial x_j}\left(A_{ij}\frac{\partial}{\partial x_i}u\right) + \sum_{k=1}^{2} B_k \frac{\partial}{\partial x_k}u + Cu, \tag{2}$$

with $A_{ij} \in L_\infty(\Omega)$, $B_k \in L_\infty(\Omega)$, $C \in L_\infty(\Omega)$, f is a function in $L_2(\Omega)$, and $g \in L^\infty(\partial\Omega)$.

When the matrix $A = [A_{ij}]_{1\le i,j\le 2}$ is symmetric and positive definite over Ω, the PDE in (1) is said to be elliptic. A typical PDE of this type can be given by defining the operator $\mathscr{L}$ with the following weight functions: Let

$$\begin{bmatrix} A_{11} & A_{12} \\ A_{21} & A_{22} \end{bmatrix} = \begin{bmatrix} \varepsilon + x & xy \\ xy & \varepsilon + y \end{bmatrix}, \tag{3}$$

with $\varepsilon > 0$, $\mathbf{B} = (B_1, B_2) = (0, 0)$, and $C = \exp(-x^2 - y^2)$. Then, the corresponding PDE is elliptic in the first quadrant. Given the conditions listed above for A_{ij}, B_k, C, f, and g, we know that this type of PDE has a unique solution. See Theorem 3 in a later section.

There is a standard approach to use methods for solution of second-order elliptic PDE to study hyperbolic equations, transport equations, and mixed parabolic and hyperbolic equations. Indeed, consider a singularly perturbed elliptic PDE:

$$-\varepsilon\Delta u + (2 - y^2)D_x u + (2 - x)D_y u + (1 + (1 + x)(1 + y)^2)u = f, \quad (x, y) \in \Omega \tag{4}$$

where $\Omega = (0, 1) \times (0, 1)$,with $u|_{\partial\Omega} = g$ where f and g are any appropriate functions. When $\varepsilon = 0$, this is a hyperbolic test problem considered in [5, 14, 15]. One can numerically solve (4) for $\varepsilon > 0$ very small to approximate the solution of the hyperbolic problem with $\varepsilon = 0$.

For another example, the following is a singularly perturbed advection-diffusion problem:

$$-\varepsilon\Delta u + D_x u + D_y u = f, \quad (x, y) \in \Omega = (0, 1) \times (0, 1), \tag{5}$$

with $u|_{\partial\Omega} = g$ where f and g are appropriate functions. This example was studied in [15].

For another example, the following problem is parabolic for $y > 0$ and hyperbolic for $y \le 0$:

$$\begin{aligned} -\varepsilon D_{yy}u + D_x u + c_1 u = 0, \quad & (x, y) \in (-1, 1) \times (0, 1), \\ D_x u + c_2 u = 0, \quad & (x, y) \in (-1, 1) \times (-1, 0], \end{aligned} \tag{6}$$

with $u|_{\partial\Omega} = g$, for any constants $c_1 > 0$ and $c_2 > 0$. It was also studied in [15]. We can use the following general elliptic PDE to study the above problem by considering

$$\begin{aligned} -\eta D_{xx}u - \varepsilon D_{yy}u + D_x u + c_1 u = f_1, \quad & (x, y) \in (-1, 1) \times (0, 1), \\ -\eta \Delta u + D_x u + c_2 u = f_2, \quad & (x, y) \in (-1, 1) \times (-1, 0], \end{aligned} \tag{7}$$

with $u|_{\partial\Omega} = g$ and $\eta > 0$ where f_1, f_2 and g are appropriate functions. We can approximate the solution to (62) by letting $\eta > 0$ go to zero and use spline functions which are not necessarily continuous at $y = 0$.

These examples show the usefulness of a numerical solution to the model problem (1) in this paper. On the other hand, it is known that not all second-order elliptic PDE has a unique solution because of the Fredholm alternative theorem (cf. e.g., [9]). Although there are many sufficient conditions to ensure the existence and uniqueness of the solution (1), it is interesting to know when such a PDE can be numerically solved and admits a numerical solution. These are our motivations to study (1). In the next section, we provide a standard sufficient condition to ensure the existence and uniqueness of the weak solution of (1) based on the Lax–Milgram theorem. The PDEs listed above may not satisfy that sufficient condition. However, we are still able to find their numerical solutions by using our polygonal splines.

This second-order elliptic PDE in (1) has been studied by many other methods before. For example, in [1], the researchers used bivariate spline method to numerically solve (1). See [21] for other numerical solutions of (1) using other spline methods. In particular, given a triangulation Δ of a domain Ω, let

$$S_d^r(\Delta) = \{s \in C^r(\Omega) : s|_T \in \mathscr{P}_d, \forall T \in \Delta\} \tag{8}$$

be the spline space of smoothness r and degree $d \ge r$. In general, we need to use $d \ge 3r + 2$ to have the spline space $S_d^r(\Delta)$ to be nonempty (cf. [16]). The researchers use $S_d^{-1}(\Delta)$ (i.e., discontinuous splines of degree d over Δ) and add the smoothness conditions $H\mathbf{c} = 0$ as side constraints to approximate the following weak solution:

$$\sum_{i,j=1}^{2} \int_\Omega A_{ij} \frac{\partial}{\partial x_i} u \frac{\partial}{\partial x_j} v + \sum_{k=1}^{2} \int_\Omega [B_k \frac{\partial}{\partial x_k} u] v + \int_\Omega Cuv = \int_\Omega fv \tag{9}$$

for all test function $v \in S_d^{-1}(\triangle)$. For another example, the researchers in [18] use the weak Galerkin method to solve (1). In this paper, we shall use the polygonal splines invented in [12] to solve (9). Polygonal splines have been shown to be more efficient than polynomial spline functions for numerical solution of the Poisson equation (cf. [12]). We shall use the polygonal splines to solve the general second-order elliptic PDE and compare the numerical solutions with the solutions by using bivariate spline functions. We continue to demonstrate that the polygonal splines numerical solutions are generally better than the ones obtained with bivariate splines of the same degrees.

This paper is organized as follows. We shall review polygonal splines in Sect. 2. Then, we review the ellipticity concept to explain when the PDE in (1) has a solution in Sect. 3. Implementation and convergence of polygonal spline solution will be explained in Sect. 4. These are generalizations of the standard results for Poisson equation: the Céa lemma and the Aubin–Nitsche technique for the optimal convergence rate in L_2 norm over a convex domain. Finally, we present many numerical results using polygonal splines to solve the PDEs given above.

2 Preliminary on Polygonal Splines

Let us begin with generalized barycentric coordinates (GBCs). There are many ways to define barycentric coordinates in a polygon with n sides, $n \geq 3$; see [10]. We will restrict our attention to convex polygons in this paper.

Let $P_n = \langle \mathbf{v}_1, \ldots, \mathbf{v}_n \rangle$ be a convex polygon. Any functions $\phi_i, i = 1, \ldots, n$, will be called generalized barycentric coordinates (GBCs) if, for all $\mathbf{x} \in P_n$, $\phi_i(\mathbf{x}) \geq 0$ and

$$\sum_{i=1}^{n} \phi_i(\mathbf{x}) = 1, \qquad \text{and} \qquad \sum_{i=1}^{n} \phi_i(\mathbf{x})\mathbf{v}_i = \mathbf{x}. \tag{10}$$

When P_n is a triangle, the coordinates ϕ_1, ϕ_2, ϕ_3 are the usual barycentric coordinates. For $n > 3$, the ϕ_i are not uniquely determined by (10), but they share the basic property that they are piecewise linear on the boundary of P_n:

$$\begin{gathered} \phi_i(\mathbf{v}_j) = \delta_{ij}, \text{ and} \\ \phi_i((1-\mu)\mathbf{v}_j + \mu\mathbf{v}_{j+1}) = (1-\mu)\phi_i(\mathbf{v}_j) + \mu\phi_i(\mathbf{v}_{j+1}) \text{ for } \mu \in [0,1]. \end{gathered} \tag{11}$$

Example 1 (*Wachspress (rational) coordinates*) For general, $n \geq 3$, let $\mathbf{n}_i \in \mathbb{R}^2$ be the outward unit normal to the edge $e_i = [\mathbf{v}_i, \mathbf{v}_{i+1}], i = 1, \ldots, n$, and for any $\mathbf{x} \in P_n$, let $h_i(\mathbf{x})$ be the perpendicular distance of $\mathbf{x}$ to the edge e_i, so that

$$h_i(\mathbf{x}) = (\mathbf{v}_i - \mathbf{x}) \cdot \mathbf{n}_i = (\mathbf{v}_{i+1} - \mathbf{x}) \cdot \mathbf{n}_i. \tag{12}$$

Let

$$w_i(\mathbf{x}) = d_i \prod_{\substack{j=1,\ldots,n \\ j\neq i-1,i}} h_j(\mathbf{x}), \text{ and } W = \sum_{j=1}^{n} w_j \tag{13}$$

where d_i is the cross product

$$d_i = \mathbf{n}_{i-1} \times \mathbf{n}_i = \begin{vmatrix} n_{i-1}^x & n_i^x \\ n_{i-1}^y & n_i^y \end{vmatrix},$$

and $\mathbf{n}_j = (n_j^x, n_j^y)$ is the normal of edge $[\mathbf{v}_i, \mathbf{v}_{i+1}]$. Then, the functions $\phi_i = w_i/W$, $i = 1, \ldots, n$ are GBCs, which are rational functions of degree $(n-2, n-3)$. See [10] for several other representations of these coordinates.

For a convex polygon P_n with $n \geq 3$ sides, let $\phi_1, \ldots, \phi_n$ be a set of GBCs. For any $d \geq 0$, and any multi-index $\mathbf{j} = (j_1, \ldots, j_n) \in \mathbb{N}_0^n$ with $|\mathbf{j}| := j_1 + \cdots + j_n = d$, let

$$B_{\mathbf{j}}^d(\mathbf{x}) = \frac{d!}{j_1! \cdots j_n!} \phi_1^{j_1}(\mathbf{x}) \cdots \phi_n^{j_n}(\mathbf{x}), \qquad \mathbf{x} \in P_n, \tag{14}$$

which we will call a Bernstein–Bézier function. Note that for $n > 3$, $B_{\mathbf{j}}^d$ is not necessarily a polynomial. For any n, define $\Phi_d(P_n)$ as the linear space of functions of the form

$$s(\mathbf{x}) = \sum_{|\mathbf{j}|=d} c_{\mathbf{j}} B_{\mathbf{j}}^d(\mathbf{x}), \qquad \mathbf{x} \in P_n, \quad c_{\mathbf{j}} \in \mathbb{R}. \tag{15}$$

The following properties are known:

1 $\Pi_d \subset \Phi_d(P_n)$ where Π_d is the space of polynomials of degree $\leq d$.
2 Due to (11), the function $s(\mathbf{x})$ in (15) is a univariate polynomial of degree $\leq d$ on each edge of the polygon.
3 When $n \geq 4$, the functions $B_{\mathbf{j}}^d \in \Phi_d(P_n)$ are not linearly independent.

Based on the polynomial blossom property, when $d = 2$ we can construct a basis for a subspace which still contains the space of quadratic polynomials Π_2:

Theorem 1 *Where $\lambda_{i,j}$, $i = 1, \ldots n$, $j \in \{-1, 0, 1\}$ is the traditional barycentric coordinate associated with $\mathbf{v}_{i+j}$ in the triangle $\langle v_{i-1}, v_i, v_{i+1}\rangle$, let*

$$F_i = \phi_i \lambda_{i,0}, \qquad F_{i,1} = \phi_i \lambda_{i,1} + \phi_{i+1} \lambda_{i+1,-1}, \qquad i = 1, \ldots, n,$$

and

$$\Psi_2(P_n) = span\{F_i, F_{i,1}, i = 1, \ldots, n\}. \tag{16}$$

Then, $\Pi_2 \subset \Psi_2(P_n) \subset \Phi_2(P_n)$.

By specializing to specifically Wachspress coordinates, we can do the same for $d \geq 3$:

Theorem 2 *For $d \geq 3$ and with Wachspress coordinates ϕ_i, let*

$$F_i = \phi_i \lambda_{i,0}^{d-1}, \qquad i = 1, ..., n,$$

$$F_{i,k} = \binom{d-1}{k} \phi_i \lambda_{i,1}^{k} \lambda_{i,0}^{d-1-k} + \binom{d-1}{k-1} \phi_{i+1} \lambda_{i+1,0}^{k-1} \lambda_{i+1,-1}^{d-k},$$

$$i = 1, ..., n, \ k = 1, ..., d-1,$$

and

$$\Psi_d(P_n) := span\{F_i, \ i = 1, ..., n\} \oplus span\{F_{i,k}, \ i = 1, ..., n, \ k = 1, ..., d-1\} \oplus \frac{b}{\sum_{j=1}^{n} w_j} \Pi_{d-3} \tag{17}$$

where b is the bubble function given by

$$b := \prod_{k=1}^{n} h_k.$$

Then, $\Pi_d \subset \Psi_d(P_n) \subset \Phi_d(P_n)$.

We refer the reader to [12] for proofs of Theorems 1 and 2.

Given a domain Ω, let $\Delta = \{P_n\}$ be a partition of Ω into convex polygons, we can use the basis elements of $\Psi_d(P_n)$ over each polygon P_n to define spline functions. For any polygons P_i, $P_j \in \Delta$, we assume that the intersection $P_i \cap P_j$ is either empty, a common edge, or a common vertex. Then, define

$$\mathcal{S}_d(\Delta) := \{s \in C(\Omega), \quad s|_{P_n} \in \Psi_d(P_n), \forall P_n \in \Delta\}. \tag{18}$$

This is the spline space we will use to numerically solve PDEs of the form (1). In particular, our numerical trials were performed when $d = 2$ and $d = 3$. In [12], it was shown that one can use the part of $\Psi_d(P_n)$ associated with the boundary of P_n, that is, span$\{F_i, \ i = 1, ..., n\} \oplus$ span$\{F_{i,k}, \ i = 1, ..., n, \ k = 1, ..., d-1\}$ to form an interpolatory basis $\{L_j, \ j = 1, ..., dn\}$:

$$\begin{aligned} L_{di-k} &= \sum_{s=1}^{d-1} r_{ks} F_{i,s}, \ \ i = 1, ..., n, \ k = 1, ..., d-1, \\ L_{di} &= F_i - \sum_{k=1}^{d-1} (1 - k/d)^d (L_{di-k} + L_{d(i-2)+k}), \ \ i = 1, ..., n \end{aligned} \tag{19}$$

where $R = (r_{ks})_{k,s=1}^{d}$ is the inverse of a matrix built from coefficients of Lagrange interpolation of univariate Bernstein polynomials of degree d. The functions L_{di} interpolate at vertices of P_n, while the functions L_{di-k} interpolate at points on edges of P_n. When $d > 3$, there is additional work to be done, as there is still another

component of the space $\Psi_d(P_n)$, namely $\frac{b}{W}\Pi_{d-3}$. Since we focus on degree 3 or less in this paper, the interested reader should refer to [12] for more information on this case.

3 Existence, Uniqueness, Stability, and Convergence of Solutions

We will review some sufficient conditions such that the elliptic PDE in (1) admits a unique weak solution with zero boundary condition, i.e., $g = 0$ on $\partial\Omega$. This PDE has been studied for a long time. We refer to [6, 7] for detail. For convenience, we include some basic theory to explain our numerical solution.

Of course, it would be beneficial to find necessary conditions as well, but these can be hard to pinpoint. In particular, it must be required that the associated homogeneous PDEs, where $f = g = 0$, have the unique solution $u = 0$; otherwise, when given a solution u^* of the PDE above, we would be able to build a distinct solution using $u^* + Ku$ for any constant K.

The weak formulation of this PDE is given by (9) for all $v \in H_0^1(\Omega)$. To do so, we shall use the following norm and semi-norm on $H^1(\Omega)$ for convenience: $\|u\|_{2,\Omega} = \|u\|_{L^2(\Omega)}$, $|u|_{1,2,\Omega} = \|\nabla u\|_{L^2(\Omega)}$, and $|u|_{2,2,\Omega} = |u|_{H^2(\Omega)}$. Similarly, $|u|_{d+1,2,\Omega} = |u|_{H^{d+2}(\Omega)}$.

Define by $a(u, v)$ the bilinear form in the left-hand side of the equation in (9). To find the weak solution in $H_0^1(\Omega)$, we must show that $a(u, v)$ is bounded above and coercive in order to use the Lax–Milgram theorem.

Definition 1 We say the PDE in (1) is uniform elliptic if the coefficient matrix $[A_{ij}]_{1\le i,j,\le 2}$ is symmetric and positive definite with smallest eigenvalue $\alpha > 0$ over Ω for a positive number α called the ellipticity of the PDE.

Theorem 3 *Suppose that the second-order PDE in (1) is uniformly elliptic with ellipticity $\alpha > 0$. Let $\beta := \|\mathbf{B}\|_{\infty,\Omega} < \infty$ and $C \ge \gamma > 0$. Suppose that there exists a positive constant c such that*

$$\alpha > \frac{\beta}{2c} \text{ and } \gamma \ge \frac{c\beta}{2}. \tag{20}$$

Then, the PDE (1) has a unique weak solution u in $H_0^1(\Omega)$ satisfying the weak formulation (9) for $v \in H_0^1(\Omega)$.

Proof A proof can be found in many standard finite element textbooks, e.g., [6, 7].

When B_1 is a function of y only and B_2 is a function of x only, we note that for all $u \in H_0^1(\Omega)$,

$$\int_\Omega B_1\left(\frac{\partial}{\partial x_1}u\right)u\,dxdy = -\int_\Omega B_1\left(\frac{\partial}{\partial x_1}u\right)u\,dxdy \tag{21}$$

by using integration by parts and zero boundary condition. Thus, $\int_\Omega B_1(\frac{\partial}{\partial x_1}u)udxdy = 0$. Similarly, $\int_\Omega B_2(\frac{\partial}{\partial x_2}u)udxdy = 0$. Hence, the terms involving first-order derivatives in $a(u,u)$ are zero and

$$\begin{aligned} a(u,u) =& \int_\Omega \left[\sum_{i,j=1}^{2} A_{ij} \frac{\partial}{\partial x_i} u \frac{\partial}{\partial x_j} u + Cu^2 \right] dxdy \\ \geq& \alpha |u|^2_{1,2,\Omega} + \gamma \|u\|^2_{2,\Omega} \end{aligned} \tag{22}$$

which implies that $a(u,u)$ is coercive. Thus, we have established the following:

Corollary 1 *Suppose that the second-order PDE in (1) is uniform elliptic with ellipticity $\alpha > 0$. Suppose that B_1 is a function of y only and B_2 is a function of x only. If $C \geq 0$, then the PDE (1) has a unique weak solution u in $H^1_0(\Omega)$ satisfying the weak formulation (9) for $v \in H^1_0(\Omega)$.*

By applying Theorem 3 and Corollary 1, we can establish the following result:

Corollary 2 *Suppose that the second-order PDE in (1) is uniform elliptic with ellipticity $\alpha > 0$. Suppose that $B_1(x,y) = \hat{B}_1(x,y) + B_1'(y)$ and $B_2(x,y) = \hat{B}_2(x,y) + B_2'(x)$ where $B_1'(y)$ is a function of y only and B_2' is a function of x only. Let $\hat{\beta} := \max\{\|\hat{B}_1\|_{\infty,\Omega}, \|\hat{B}_2\|_{\infty,\Omega}\} < \infty$ and $C \geq \gamma > 0$. Suppose that there exists a positive constant c such that*

$$\alpha > \frac{\hat{\beta}}{2c} \text{ and } \gamma \geq \frac{c\hat{\beta}}{2}. \tag{23}$$

Then, the PDE (1) has a unique weak solution u in $H^1_0(\Omega)$ satisfying the weak formulation (9) for $v \in H^1_0(\Omega)$.

In particular, when $B_1 = B_2 \equiv 0$, the PDE in (1) has a unique weak solution according to Theorem 3 and Corollary 2. In fact, we can establish the existence, uniqueness, and stability of the solution of (1) without using Lax–Milgram theorem. Indeed, in this case, it is easy to see that the weak form $a(u,v) = \langle f, v\rangle$ is the Euler–Langrange equation of the following minimization:

$$\min_{\substack{u \in H^1(\Omega) \\ u|_{\partial\Omega} = g}} J_f(u) \tag{24}$$

where $J_f(u) = \frac{1}{2}a(u,u) - \langle f, u\rangle$. To approximate the exact solution $u \in H^1(\Omega)$ with $u|_{\partial\Omega} = 0$, we can instead find the minimum among $u \in H^1_0(\Omega)$. To numerically solve the PDE, we can instead search for u in $\mathcal{S}_d := H^1_0(\Omega) \cap S_d(\Delta)$ where $S_d(\Delta)$ is the space of polygonal splines of order d which are defined with respect to a polygonal partition Δ of Ω as explained in the previous section. In the following analysis, we will consider this minimization for $u \in \mathcal{S}_d$.

Using a standard convex analysis, one can show

Theorem 4 *Suppose that* $[A_{ij}]_{1\le i,j\le 2}$ *is symmetric and positive definite. Suppose that* $B_1 = B_2 \equiv 0$. *If* $C \ge \gamma \ge 0$, *then* J_f *is strongly convex with convexity coefficient* μ *which is independent of* f*; therefore,* J_f *has a unique minimizer* u_f. *Hence, there exists a unique weak solution* u_f *satisfying (9).*

We can further derive the following result regarding the stability of the minimizer of J_f with respect to the source function f:

Theorem 5 *Suppose that the PDE in (1) satisfies the uniform ellipticity conditions in the hypotheses of Theorem 3. For two functions* f *and* g, *denote the minimizer of* J_f *by* u_f *and the minimizer of* J_g *by* u_g. *Then* $||u_f - u_g||_{L^2(\Omega)} \le \mu^{-1}||f - g||_{L^2(\Omega)}$.

Proof Since J_f and J_g are both μ-strongly convex, we can say that

$$J_f(u_g) - J_f(u_f) \ge \langle \nabla J_f(u_f), u_g - u_f\rangle + \frac{\mu}{2}||u_f - u_g||^2_{L^2(\Omega)} = \frac{\mu}{2}||u_f - u_g||^2_{L^2(\Omega)}$$

and

$$J_g(u_f) - J_g(u_g) \ge \langle \nabla J_g(u_g), u_f - u_g\rangle + \frac{\mu}{2}||u_f - u_g||^2_{L^2(\Omega)} = \frac{\mu}{2}||u_f - u_g||^2_{L^2(\Omega)}$$

where the last equalities in each equation come from the fact that u_f and u_g minimizing J_f and J_g, respectively, implies that both $\nabla J_f(u_f)$ and $\nabla J_g(u_g)$ are 0. If we sum two equations above, then after some simplification we see that

$$\langle f - g, u_f - u_g\rangle \ge \mu||u_f - u_g||^2_{L^2(\Omega)}.$$

Using Cauchy–Schwarz on the left side of this inequality gives us

$$||f - g||_{L^2(\Omega)}||u_f - u_g||_{L^2(\Omega)} \ge \mu||u_f - u_g||^2_{L^2(\Omega)}.$$

A simple division by $\mu||u_f - u_g||_{L^2(\Omega)}$ yields the desired result.

Finally, we discuss convergence of the numerical solutions. The discussion is divided into two parts. The first part shows the approximation power of $\mathscr{S}_d(\Delta)$. The second part is to apply the approximation property to establish the convergence of polygonal splines to the weak solution.

Proving the approximation power of this space is more complicated than in the cases of finite elements and splines over triangulations due to difficulties in bounding the gradients of the Wachspress coordinates. Fortunately, it has been shown in [10, 11] that

$$\sup_{\mathbf{x}\in P}\sum_{j=1}^{n}||\nabla\phi_j(\mathbf{x})||_2 \le \frac{4}{h_*} \tag{25}$$

where h^* is the shortest perpendicular distance from any vertex of P to a nonincident edge of P. To control this quantity, we will have to assume that Δ satisfies

$$0 < \alpha_1 < \theta_{P,i} < \alpha_2 < \pi, \quad i = 1, \cdots, n(P), \forall P \in \Delta \tag{26}$$

for two given positive constants α_1 and α_2 where $\theta_{P,i}$ is the interior angle of P at its ith vertex, and $n(P)$ stands for the number of sides of P. We shall assume that there exists a positive integer n_0 such that $n(P) \le n_0$ for all $P \in \Delta$. For each $P \in \Delta$, let $|P|$ be the diameter of P, that is, the diameter of the smallest circle containing P and ρ_P be the radius of the largest circle contained in P. We use $\kappa_P = \frac{|P|}{\rho_P}$ to be the shape parameter of P (cf. [16]) or the chunkiness of P (cf. [7]). For convenience, we let $|\Delta|$ be the largest of $|P|$ for all $P \in \Delta$ instead of the longest of the lengths of edges of Δ which is commonly used for triangulations. Where $e(P)$ is the length of the shortest edge of P, let $e(\Delta) = \min\{e(P), P \in \Delta\}$. We will assume that the global shape parameter γ_Δ to satisfy

$$\gamma_\Delta = \frac{|\Delta|}{e(\Delta)} \le \gamma < \infty \tag{27}$$

in the following study for a given $\gamma > 0$.

As $\mathcal{S}_d(\Delta)$ is a space of continuous functions over Ω, we cannot simply apply the Bramble–Hilbert lemma to establish the approximation property of $\mathcal{S}_d(\Delta)$. Instead, we follow the ideas in [16]. For simplicity, let us focus ourselves to the case $d = 2$; the case $d \ge 3$ can be done similarly.

First, we prove the following:

Lemma 1 *Let P be an n-gon in Δ. Let L_j be one of the functions listed in (19) which is supported on P. Then*

$$||L_j||_{2,P} \le C_{n,\alpha_2,\gamma}|P| \tag{28}$$

and

$$|L_j|_{1,2,P} \le C_{n,\alpha_1,\alpha_2,\gamma} \tag{29}$$

for two positive constants $C_{n,\alpha_2,\gamma}$ and $C_{n,\alpha_1,\alpha_2,\gamma}$.

Proof Since the functions L_j are built from linear combinations of the functions F_k and $F_{k,1}$ given in Theorem 1, we have for some constant C_n which depends only on n

$$||L_j||_{2,P} \le C_n \max_{k=1,\ldots,n}\{||F_k||_{2,P}, ||F_{k,1}||_{2,P}\}.$$

Thus, we really need to bound $||F_k||_{2,P}$ and $||F_{k,1}||_{2,P}$. By the definition of F_k,

$$||F_k||_{2,P} \le ||\phi_i\lambda_{i,0}||_{2,P} \le ||\lambda_{i,0}||_{\infty,P}||\phi_i||_{2,P} \le |P|||\lambda_{i,0}||_{\infty,P}.$$

To estimate $||\lambda_{i,0}||_{\infty,P}$, let $h_{\perp,i}$ be the perpendicular distance from $\mathbf{v}_i$ to the line connecting $\mathbf{v}_{i-1}$ to $\mathbf{v}_{i+1}$, and denote by m_i the point on this line which is a distance $h_{\perp,i}$ from $\mathbf{v}_i$. Then since $\lambda_{i,0}$ is a linear function, we have $||\nabla\lambda_{i,0}||_2 = \frac{1}{h_{\perp,i}}$.

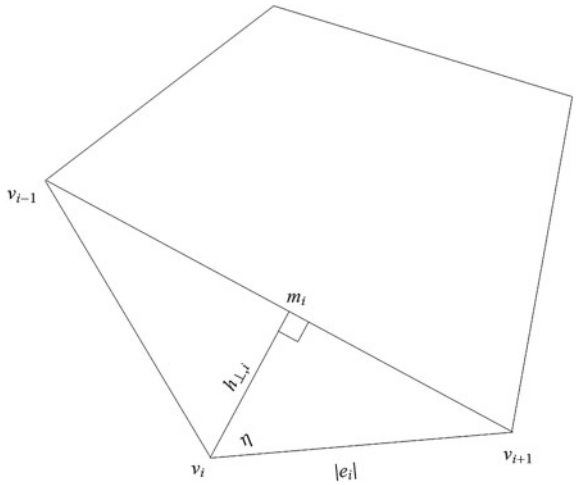

Fig. 1 An illustration to clarify the geometry used to show (30)

Let $|e_{i-1}|$ be the length of the edge between $\mathbf{v}_{i-1}$ and $\mathbf{v}_i$ and similar for $|e_i|$. Without loss of generality, suppose that $|e_i| \leq |e_{i-1}|$. If we draw the triangle $\tau = \langle \mathbf{v}_i, \mathbf{v}_{i+1}, m_i \rangle$ (see Fig. 1), we can see that $h_{\perp,i} = |e_i| \cos \eta$ where η is the interior angle of τ at $\mathbf{v}_i$. Since $|e_i| \leq |e_{i-1}|$, we have that $\eta < \frac{1}{2}\theta_{P,i}$. By (26), $0 < \frac{1}{2}\theta_{P,i} < \frac{\pi}{2}$, so

$$\cos \eta \geq \cos(\frac{1}{2}\theta_{P,i}) = \sqrt{\frac{1+\cos\theta_{P,i}}{2}} \geq \sqrt{\frac{1+\cos\alpha_2}{2}} = C_{\alpha_2} \tag{30}$$

for a constant C_{α_2} which depends on α_2.

Therefore, we have that

$$h_{\perp,i} \geq C_{\alpha_2}|e_i| \geq C_{\alpha_2} e(P). \tag{31}$$

Now, $||\lambda_{i,0}||_{\infty,P}$ will be achieved by $\lambda_{i,0}$ at the point in P which has the largest perpendicular distance from the line connecting $\mathbf{v}_{i-1}$ and $\mathbf{v}_{i+1}$, which is of course a distance at most $|P|$ from this line. Since $\lambda_{i,0}$ is linear, we have that

$$||\lambda_{i,0}||_{\infty,P} \leq \frac{|P|}{h_{\perp,i}} \leq \frac{1}{C_{\alpha_2}} \frac{|P|}{e(P)} \leq C_{\alpha_2}\gamma. \tag{32}$$

Therefore, we have $||F_k||_{2,P} \leq C_{n(P),\alpha_2,\gamma}|P|$. A similar argument shows that

$$||F_{k,1}||_{2,P} \leq \frac{2}{C_2} \frac{|P|^2}{e(P)} \leq C_{n,\alpha_2,\gamma}|P|,$$

which completes the proof of (28).

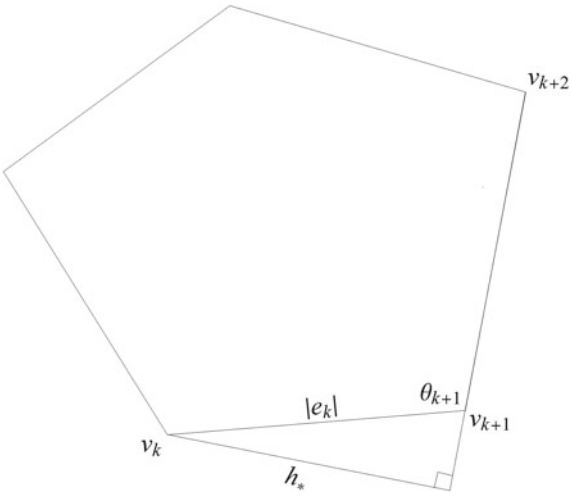

Fig. 2 An illustration of the geometry used to show (33)

To prove (29), we will follow a similar strategy. As

$$|L_j|_{1,2,P} \leq C_n \max_{k=1,\ldots,n} \{|F_k|_{1,2,P}, |F_{k,1}|_{1,2,P}\},$$

we need to bound $|F_k|_{1,2,P}$ and $|F_{k,1}|_{1,2,P}$.

$$\begin{aligned}
|F_k|^2_{1,2,P} &= \int_P (\lambda_{i,0} D_x \phi_i + \phi_i D_x \lambda_{i,0})^2 + (\lambda_{i,0} D_y \phi_i + \phi_i D_y \lambda_{i,0})^2 \, dx \, dy \\
&\leq 2 \sup_{\mathbf{x}\in P} ||\nabla \phi_i(\mathbf{x})||_2^2 \int_P \lambda_{i,0}^2 \, dx \, dy + 2 \sup_{\mathbf{x}\in P} ||\nabla \lambda_{i,0}(\mathbf{x})||_2^2 \int_P \phi_i^2 \, dx \, dy \\
&\leq 2 \sup_{\mathbf{x}\in P} ||\nabla \phi_i(\mathbf{x})||_2^2 (||\lambda_{i,0}||^2_{\infty,P}) |P|^2 + \tfrac{2}{h^2_{\perp,i}} |P|^2 \\
&\leq C_{n(P)} \sup_{\mathbf{x}\in P} ||\nabla \phi_i(\mathbf{x})||_2^2 \left(\tfrac{|P|}{h_{\perp,i}}\right)^2 |P|^2 + C_{n(P)} \left(\tfrac{|P|}{h_{\perp,i}}\right)^2 \\
&\leq C_{n(P)} \tfrac{16|P|^2}{h_*^2} \left(\tfrac{|P|}{h_{\perp,i}}\right)^2 + C_{n(P)} \left(\tfrac{|P|}{h_{\perp,i}}\right)^2 = C_{n(P),\alpha_2} \left(\tfrac{|P|}{e(P)}\right)^2 (1 + \tfrac{16|P|^2}{h_*^2})
\end{aligned}$$

by using (25) and (31).

Now, we will show that h_* is comparable to $e(P)$. In particular, since P is convex, h_* ought to be realized by a line drawn from a vertex of P, say v_k, to an edge to an edge which is a graph-distance of 2 from v_k, say the edge between v_{k+1} and v_{k+2}. If we draw in this line (see Fig. 2), a right triangle is formed which shows that

$$h_* = \sin\theta_{k+1} |e_k| \geq \min_{\mathbf{x}} \{\sin\alpha_1, \sin\alpha_2\} e(P). \tag{33}$$

Therefore, we can say

$$\sup_{\mathbf{x}\in P} ||\nabla\phi_i(\mathbf{x})||_2^2 \leq \frac{16}{h_*^2} \leq \frac{C_{\alpha_1,\alpha_2}}{e(P)^2}. \tag{34}$$

Combining (34) and our above analysis shows that

$$\begin{aligned} |F_k|_{1,2,P}^2 &\leq C_{n(P)} \tfrac{|P|^2}{e(P)^2}(1 + 16C_{\alpha_1,\alpha_2}\tfrac{|P|^2}{e(P)^2}) \\ \Rightarrow |F_k|_{1,2,P} &\leq C_{\alpha_1,\alpha_2}\tfrac{|P|}{e(P)}(1 + \tfrac{|P|}{e(P)})C_{\alpha_1,\alpha_2,\gamma}. \end{aligned}$$

A similar argument will show that $|F_{k,1}|_{1,2,P} \leq C_{\alpha_1,\alpha_2,\gamma}$, so we have that $|L_j|_{1,2,P} \leq C_{n,\alpha_1,\alpha_2,\gamma}$ as desired in (29).

We are nearly ready to establish the approximation power of $\mathscr{S}_d(\Delta)$. Our main result is the following theorem:

Theorem 6 *Suppose that Δ satisfies four assumptions: $\gamma_\Delta \leq \gamma$, $0 < \alpha_1 \leq \theta_{P,i} \leq \alpha_2 < \pi$, $\kappa_P \leq \kappa < \infty$ and $n(\Delta) \leq n_0$. Then for any $u \in H^{d+1}(\Omega)$, there exists a polygonal spline $Q(u) \in \mathscr{S}_d(\Delta)$ such that*

$$\|u - Q(u)\|_{2,\Omega} \leq C_{n_0,\alpha_1,\alpha_2,\kappa,\gamma}|\Delta|^{d+1}|u|_{d+1,2,\Omega} \tag{35}$$

and

$$|u - Q(u)|_{1,2,\Omega} \leq C_{n_0,\alpha_1,\alpha_2,\kappa,\gamma}|\Delta|^{d}|u|_{d+1,2,\Omega} \tag{36}$$

for constant $C(n_0, \alpha_1, \alpha_2, \kappa, \gamma)$ which is independent of u and $|\Delta|$, but may depend on the domain Ω if Ω is nonconvex.

Similarly, for any $u \in H^{d+1}(\Omega) \cap H_0^1(\Omega)$, there exists a polygonal spline $Q_0(u) \in \mathscr{S}_d(\Delta) \cap H_0^1(\Omega)$ such that

$$\|u - Q_0(u)\|_{2,\Omega} \leq C_{n_0,\alpha_1,\alpha_2,\kappa,\gamma}|\Delta|^{d+1}|u|_{d+1,2,\Omega} \tag{37}$$

and

$$|u - Q_0(u)|_{1,2,\Omega} \leq C_{n_0,\alpha_1,\alpha_2,\kappa,\gamma}|\Delta|^{d}|u|_{d+1,2,\Omega} \tag{38}$$

for another constant $C(n_0, \alpha_1, \alpha_2, \kappa, \gamma)$ which is independent of u and $|\Delta|$, but may depend on the domain Ω if Ω is nonconvex.

We will require bit more discussion, along with another lemma, to prove this theorem. For convenience, we consider the case $d = 2$ first. Let us recall locally supported basis functions in $\mathscr{S}_d(\Delta)$ from [12]. For each vertex $\mathbf{v} \in \Delta$, let $L_v \in \mathscr{S}_2(\Delta)$ be the spline supported on the collection $\Omega_\mathbf{v}$ of polygons which has $\mathbf{v}$ as one of its vertices satisfying $L_v(\mathbf{v}) = 1$ and zero for other vertices and zero for all midpoints of edges. For each edge $e \in \Delta$, let $L_e \in \mathscr{S}_2(\Delta)$ be the spline supported on the collection Ω_e of polygons which share the edge e satisfying $L_e(\mathbf{w}_e) = 1$ and zero for all vertices and zero for all midpoints of other edges where $\mathbf{w}_e$ is the midpoint of e. By the definition of these locally supported polygonal splines, we have that

$$\mathcal{S}_2(\Delta) = \text{span}\{L_v, \forall \mathbf{v} \in \Delta\} \oplus \text{span}\{L_e, \forall e \in \Delta\}.$$

We will construct quasi-interpolatory splines $Q(u) \in \mathcal{S}_2(\Delta)$ and $Q_0(u) \in \mathcal{S}_2(\Delta) \cap H_0^1(\Omega)$.

To this end, we first extend any $u \in H^3(\Omega)$ to a function in $H^3(\mathbb{R}^2)$ with the property $\|u\|_{H^3(\mathbb{R}^2)} \le E\|u\|_{H^3(\Omega)}$ with a positive constant E dependent only on Ω (cf. [22]) and call it u again for convenience.

For each $\mathbf{v}$, let $\Omega_{\mathbf{v}}$ be the collection of all polygons sharing the vertex $\mathbf{v}$. Let $B_{\mathbf{v}}$ be largest disk contained in $\Omega_{\mathbf{v}}$ if $\mathbf{v}$ is an interior vertex. If $\mathbf{v}$ is a boundary vertex, we let $B_{\mathbf{v}}$ be the largest disk contained in the convex hull $co(\Omega_{\mathbf{v}})$ of $\Omega_{\mathbf{v}}$. Let $F_{\mathbf{v}}(u)$ is the averaged Taylor polynomial of degree 2 associated with u based on the disk $B_{\mathbf{v}}$ (cf. [16]). Define by

$$c_{\mathbf{v}}(u) = F_{\mathbf{v}}(u)|_{\mathbf{v}}. \tag{39}$$

Let $T_{\mathbf{v}} \in \Omega_{\mathbf{v}}$ be a triangle with a vertex $\mathbf{v}$. We simply use the polynomial property $\|p\|_{\infty,T} \le \frac{K_1}{|T|}\|p\|_{2,T}$ for any triangle T along with the property that $\|F_{\mathbf{v}}(u)\|_{2,co(\Omega_{\mathbf{v}})} \le K_2\|u\|_{2,co(\Omega_{\mathbf{v}})}$ (cf. [16]) to have

$$|c_{\mathbf{v}}(u)| \le \|F_{\mathbf{v}}(u)\|_{\infty,T} \le \frac{K_1}{|T_{\mathbf{v}}|}\|F_{\mathbf{v}}(u)\|_{2,T} \le \frac{K_1K_2}{|T_{\mathbf{v}}|}\|u\|_{2,co(\Omega_{\mathbf{v}})} \tag{40}$$

for two constants K_1 and K_2 independent of u and $T_{\mathbf{v}}$. Similarly, for $e \in \Delta$, let Ω_e be the union of two polygons in Δ if e is an interior edge. Let B_e be a largest disk contained in Ω_e. If e is a boundary edge, we can choose a disk B_e contained in the polygon with edge e. Then we let $F_e(u)$ be the averaged Taylor polynomial of degree d based on B_e. Choose c_e to be the value at $F_e(u)$ evaluated at the midpoint $\mathbf{w}_e$ of e. Choose a good triangle T_e containing $\mathbf{w}_e$. Then, $c_e(u)$ will satisfy a similar property in (40). Our quasi-interpolatory spline is defined by

$$Q(u) = \sum_{\mathbf{v}\in\Delta} c_{\mathbf{v}}(u)L_v + \sum_{e\in\Delta} c_e(u)L_e. \tag{41}$$

Similarly, for $u \in H_0^1(\Omega)$, we let

$$Q_0(u) = \sum_{\substack{\mathbf{v}\in\Delta\\ \mathbf{v}\notin\partial\Omega}} c_{\mathbf{v}}(u)L_v + \sum_{\substack{e\in\Delta\\ e\notin\partial\Omega}} c_e(u)L_e. \tag{42}$$

Thus, $Q_0(u) \in \mathcal{S}_d(\triangle) \cap H_0^1(\Omega)$. Let us show that $Q(u)$ and $Q_0(u)$ are bounded operators on $L^2(\Omega)$. That is,

Lemma 2 *For any $u \in L^2(\Omega)$, we have*

$$\|Q(u)\|_{2,\Omega} \le K_3\|u\|_{2,\Omega} \tag{43}$$

for a positive constant K_3 independent of u. In addition, for nonnegative integers α, β with $\alpha + \beta = 1$,

$$\|D_x^\alpha D_y^\beta Q(u)\|_{2,\Omega} \leq \frac{K_4}{e(\Delta)}\|u\|_{2,\Omega} \tag{44}$$

for another positive constant K_4 independent of u. The same estimates hold for Q_0.

Proof For each polygon $P \in \Delta$, denote by Ω_P the union of polygons which share an edge or a vertex of P. Note that $L_{\mathbf{v}}|_P$ is just L_j for some j and so is $L_e|_P$. Then, we use Lemma 1 to have

$$\begin{aligned}
\|Q(u)\|_{2,P} &= \left[\int_P |\sum_{\mathbf{v}\in P} c_{\mathbf{v}}(u)L_v + \sum_{e\in P} c_e(u)L_e|^2 dx\, dy\right]^{1/2} \\
&\leq \sum_{\mathbf{v}\in P} |c_{\mathbf{v}}(u)| \left(\int_P |L_v|^2 dx\, dy\right)^{1/2} + \sum_{e\in P} |c_e(u)| \left(\int_P |L_e|^2 dx\, dy\right)^{1/2} \\
&\leq \sum_{\mathbf{v}\in P} \frac{K_1K_2}{|T_{\mathbf{v}}|}\|u\|_{2,\Omega_{\mathbf{v}}}||L_v||_{2,P} + \sum_{e\in P} \frac{K_1K_2}{|T_e|}\|u\|_{2,\Omega_e}||L_e||_{2,P} \\
&\leq C_{n(P),\alpha_2,\gamma} \frac{|P|}{\min\limits_{\mathbf{v},e\in P}\{|T_{\mathbf{v}}|, |T_e|\}}||u||_{2,\Omega_P} \\
&\leq C_{n_0,\alpha_2,\gamma} \frac{|\Delta|}{e(\Delta)}||u||_{2,\Omega_P} \leq C_{n_0,\alpha_2,\gamma}||u||_{2,\Omega_P}
\end{aligned}$$

for a constant $C_{n_0,\alpha_2,\gamma}$ as we are always able to choose $|T_{\mathbf{v}}| \geq e(P)$ and $|T_e| \geq e(P)$. Hence,

$$\begin{aligned}
\|Q(u)\|_{2,\Omega}^2 &= \sum_{P\in\Delta} \|Q(u)\|_{2,P}^2 \leq C_{n_0,\alpha_2,\gamma}^2 \sum_{P\in\Delta} ||u||_{2,\Omega_P}^2 \\
&\leq C_{n_0,\alpha_1,\alpha_2,\gamma}^2 \sum_{P\in\Delta} \|u\|_{2,P}^2 = C_{n_0,\alpha_1,\alpha_2,\gamma}^2 \|u\|_{2,\Omega}^2
\end{aligned} \tag{45}$$

where we have used the fact that $\sum_{P\in\Delta} ||u||_{2,\Omega_P}^2 \leq C(n_0,\alpha_1)\sum_{P\in\Delta} ||u||_{2,p}^2$ for a positive constant $C(n_0,\alpha_1)$ since for each polygon $q \in \Delta$, $q \in \Omega_P$ for at most $n_0 2\pi/\alpha_1$ polygons $P \in \Delta$.

Similarly, for nonnegative integers α and β such that $\alpha + \beta = 1$, we have

$$\|D_x^\alpha D_y^\beta Q(u)\|_{2,P} = \left[\int_P |\sum_{\mathbf{v}\in P} c_{\mathbf{v}}(u) D_x^\alpha D_y^\beta L_v + \sum_{e\in P} c_e(u) D_x^\alpha D_y^\beta L_e|^2 dxdy\right]^{1/2}$$
$$\le \sum_{\mathbf{v}\in P} |c_{\mathbf{v}}(u)| \left(\int_P |D_x^\alpha D_y^\beta L_v|^2\right)^{1/2} + \sum_{e\in P} |c_e(u)| \left(\int_P |D_x^\alpha D_y^\beta L_e|^2 dxdy\right)^{1/2}$$
$$\le \sum_{\mathbf{v}\in P} \frac{K_1K_2}{|T_{\mathbf{v}}|}\|u\|_{2,\Omega_{\mathbf{v}}}|L_{\mathbf{v}}|_{1,2,\Omega_{\mathbf{v}}} + \sum_{e\in P} \frac{K_1K_2}{|T_e|}\|u\|_{2,\Omega_e}|L_e|_{1,2,\Omega_e}$$
$$\le C_{n_0,\alpha_1,\alpha_2,\gamma} \frac{||u||_{2,\Omega_P}}{e(\Delta)}.$$

Hence, we have

$$\|D_x^\alpha D_y^\beta Q(u)\|_{2,\Omega}^2 = \sum_{P\in\Delta} \|D_x^\alpha D_y^\beta Q(u)\|_{2,P}^2$$
$$\le C_{n_0,\alpha_2,\gamma}^2 \sum_{P\in\Delta} ||u||_{2,\Omega_P}^2 \frac{1}{e(\Delta)^2} = \frac{C_{n_0,\alpha_1,\alpha_2,\gamma}^2}{e(\Delta)^2}\|u\|_{2,\Omega}^2. \tag{46}$$

By taking the square root both sides, we finish the proof of (44).

Similarly, we have the same estimates for Q_0.

Now, we are ready to prove the main result:

Proof (*of Theorem* 6) For simplicity, let us consider the approximation in $L^2(\Omega)$ first. It is easy to see

$$\|u - Q(u)\|_{L^2(\Omega)}^2 = \sum_{P\in\Delta} \|u - Q(u)\|_{L^2(P)}^2$$
$$\le 2\sum_{P\in\Delta} \|u - F_{P,2}(u)\|_{L^2(P)}^2 + \|F_{P,2}(u) - Q(u)\|_{L^2(P)}^2 \tag{47}$$

where $F_{P,2}(u)$ is the averaged Taylor polynomial of degree 2 associated with u based on the largest disk B_P inside P. We know from [16] that

$$||u - F_{P,2}(u)||_{2,P} \le C_{\kappa_P}|P|^3|u|_{3,2,P}. \tag{48}$$

For $\mathbf{v} \in P$, $F_{\mathbf{v}}(F_{P,2}(u)) = F_{P,2}(u)$ and for $e \in P$, $F_e(F_{P,2}(u)) = F_{P,2}(u)$. we have $Q(F_{P,2}(u)) = F_{P,2}(u)$, and hence, by Lemma 2,

$$\|F_{P,2}(u) - Q(u)\|_{2,P} = \|Q(F_{P,2}(u) - u)\|_{2,P}$$
$$\le K_3\|u - F_{P,2}(u)\|_{2,\Omega_P} \le K_3C_{\kappa_P}|\Omega_P|^3|u|_{3,2,\Omega_P}.$$

Combining this with (47) and (48), we have the following:

$$\begin{aligned}\|u - Q(u)\|^2_{2,\Omega)} &\le 2\sum_{P\in\Delta} ||u - F_{P,2}(u)||^2_{2,P} + \|F_{P,2}(u) - Q(u)\|^2_{2,P} \\ &\le \sum_{P\in\Delta} C^2_{\kappa_P}|P|^6|u|^2_{3,2,P} + K^2C^2_{\kappa_P}|\Omega_P|^6|u|^2_{3,2,\Omega_P} \\ &\le K_3^2(1 + C_\kappa^2)\sum_{P\in\Delta}|\Omega_P|^6|u|^2_{3,2,\Omega} \le K_3^2(1 + C_\kappa^2)|\Delta|^6|u|^2_{3,2,\Omega}\end{aligned}$$

where we have noted that the number of polygons containing each vertex is bounded by $2\pi/\alpha_1$, and hence, the number of polygons $p \in \Delta$ such that $p \subset \Omega_P$ is bounded by $n_0 2\pi/\alpha_1$ and that $|\Omega_P| \le 3|\Delta|$. Therefore,

$$||u - Q(u)||_{2,\Omega} \le C_\kappa|\Delta|^3|u|_{3,2,\Omega}.$$

Now, we consider $|u - Q(u)|_{1,2,\Omega}$. Recall that the averaged Taylor polynomial has the property that $D_x^\alpha D_y^\beta F_{P,d}(u) = F_{P,d-\alpha-\beta}(D_x^\alpha D_y^\beta u)$, so we use Lemma 2, i.e., (44) to have

$$\begin{aligned}&|u - Q(u)|^2_{1,2,\Omega} = \sum_{\alpha+\beta=1} ||D_x^\alpha D_y^\beta(u - Q(u))||^2_{2,\Omega} \\ &= \sum_{P\in\Delta}\sum_{\alpha+\beta=1} ||D_x^\alpha D_y^\beta(u - Q(u))||^2_{2,P} \\ &\le 2\sum_{P\in\Delta}\sum_{\alpha+\beta=1} ||D_x^\alpha D_y^\beta u - F_{P,1}(D_x^\alpha D_y^\beta u)||^2_{2,P} + ||D_x^\alpha D_y^\beta(F_{P,1}(u) - Q(u))||^2_{2,P} \\ &= 2\sum_{P\in\Delta}\sum_{\alpha+\beta=1} ||D_x^\alpha D_y^\beta u - F_{P,1}(D_x^\alpha D_y^\beta u)||^2_{2,P} + \frac{K_4^2}{e(\Delta)^2}\|F_{P,2}(u) - u||^2_{2,\Omega_P} \\ &\le 2\sum_{P\in\Delta}\sum_{\alpha+\beta=1} C_{\kappa_P}|P|^4|D_x^\alpha D_y^\beta u|^2_{2,2,\Omega_P} + \frac{K_4^2}{e(\Delta)^2}C_{\kappa_P}|P|^6|u|^2_{3,\Omega_P}\end{aligned}$$

which completes the proof of (36).

To prove (37), we have

$$\|u - Q_0(u)\|^2_{2,\Omega} \le 2\|u - Q(u)\|^2_{2,\Omega} + 2\|Q(u) - Q_0(u)\|^2_{2,\Omega}. \tag{49}$$

We use (35) for the first term on the right-hand side. Let us focus on the second term. Note from (41)

$$Q(u) - Q_0(u) = \sum_{\mathbf{v}\in\partial\Omega} c_\mathbf{v}(u)L_\mathbf{v} + \sum_{e\in\partial\Omega} c_e(u)L_e.$$

From (39), we have $c_\mathbf{v}(u) = F_\mathbf{v}(u)|_\mathbf{v} = (F_\mathbf{v}(u) - u)|_\mathbf{v}$ since $u = 0$ on $\partial\Omega$. Thus, $|c_\mathbf{v}(u)| \le \|F_\mathbf{v}(u) - u\|_{\infty,co(\Omega_\mathbf{v})}$. Using the estimate on page 9 of [16] and letting $q \to \infty$, we have

$$\|u - F_{\mathbf{v}}(u)\|_{\infty,co(\Omega_{\mathbf{v}})} \le \frac{K}{2}(1+\kappa_{co(\Omega_{\mathbf{v}})}) \sum_{\alpha+\beta=3} \frac{3!}{\alpha!\beta!} \times$$

$$\| \int_{\langle (x,y),B_{\mathbf{v}}\rangle} |D_\nu^\alpha D_\mu^\beta u(\nu,\mu)|[(x-\mu)^2+(y-\nu)^2]^{1/2} d\nu d\mu \|_{\infty,co(\Omega_{\mathbf{v}})}$$

$$\le K_8 |\Omega_{\mathbf{v}}| \sum_{\alpha+\beta=3} \int_{\Omega_{\mathbf{v}}} |D_\nu^\alpha D_\mu^\beta u(\nu,\mu)| d\nu d\mu \le K_8 |\Omega_{\mathbf{v}}|^2 |u|_{3,2,co(\Omega_{\mathbf{v}})}$$

where we have used the Cauchy–Schwarz inequality in the last inequality and $K_8 > 0$ is a constant independent of u and $|\Delta|$. We can use a similar estimate for $c_e(u)$. Hence, due to the boundedness of $L_{\mathbf{v}}$ and L_e, we conclude

$$\begin{aligned}
\|Q(u) - Q_0(u)\|_{2,\Omega}^2 &\le 2 \sum_{\substack{P\in\Delta \\ P\cap\partial\Omega\neq\emptyset}} \| \sum_{\mathbf{v}\in P\cap\partial\Omega} c_{\mathbf{v}}(u) L_{\mathbf{v}}\|_{2,P}^2 + \| \sum_{e\in P\cap\partial\Omega} c_e(u) L_e\|_{2,P}^2 \\
&\le 2 \sum_{\mathbf{v}\in\partial\Omega} K_8^2 |\Omega_{\mathbf{v}}|^4 |u|_{3,2,co(\Omega_{\mathbf{v}})}^2 \|L_{\mathbf{v}}\|_{2,co(\Omega_{\mathbf{v}})}^2 \\
&\quad + 2 \sum_{e\in\partial\Omega} K_8^2 |\Omega_e|^4 |u|_{3,2,\Omega_e}^2 \|L_e\|_{2,\Omega_e}^2 \\
&\le K_9 |\Delta|^6 |u|_{3,2,\Omega}^2
\end{aligned}$$

by using Lemma 1 where $K_9 > 0$ is a constant independent of u. This finishes the estimate for the second term in (49) and hence, the estimate in (37) follows.

The estimate in (38) is derived similarly.

Theorem 7 *Suppose that the PDE in (1) satisfies the assumptions in Theorem 3 and Δ satisfies (27) and (26). Suppose that the weak solution u of the PDE in (1) is in $H^{d+1}(\Omega)$. Let $u_S \in \mathscr{S}_d$ be the weak solution satisfying $a(u_S, v) = \langle f, v\rangle$ for all $v \in \mathscr{S}_d$. Then*

$$|u - u_S|_{1,2,\Omega} \le K |u|_{d+1,2,\Omega} |\Delta|^d \tag{50}$$

where $|\Delta|$ is the length of the longest edge in Δ, and $K = K(\Omega, \Delta, A, \mathbf{B}, C)$ is a positive constant depending only on the domain Ω, the partition Δ, the largest eigenvalue Λ of A and $\|C\|_{\infty,\Omega}$.

Proof We must prove some preliminary results in order to prove the results in this theorem. First, notice that in the proof of Theorem 3, we actually have

$$a(v,v) \ge \mu |v|_{1,2,\Omega}^2 \tag{51}$$

where $\mu = \alpha - \dfrac{c\beta}{2}$ for $c > 0$ such that $\gamma - \dfrac{\beta}{2c} \ge 0$. In addition, we can show that $a(u,v)$ is bounded. Indeed,

$$
\begin{aligned}
a(u,v) &= \int_{\Omega} \sum_{i,j=1}^{2} A_{ij} \frac{\partial u}{\partial x_i} \frac{\partial v}{\partial x_j} + \int_{\Omega} \sum_{k=1}^{2} B_k \frac{\partial u}{\partial x_k} v + \int_{\Omega} Cuv \\
&\le \Lambda ||\nabla u||_{L^2} ||\nabla v||_{L^2} + \beta ||\nabla u||_{L^2} ||v||_{L^2} + \|C\|_{\infty} ||u||_{L^2} ||v||_{L^2} \\
&\le M_1 \left(||\nabla u||_{L^2} ||\nabla v||_{L^2} + ||\nabla u||_{L^2} ||v||_{L^2} + ||u||_{L^2} ||v||_{L^2} \right) \\
&\le M_1 \left(|u|_{1,2,\Omega} |v|_{1,2,\Omega} + |u|_{1,2,\Omega} (K_1 |v|_{1,2,\Omega}) + (K_1 |u|_{1,2,\Omega})(K_1 |v|_{1,2,\Omega}) \right) \\
&\le 3 \max\{M_1, M_1 K_1, M_1 K_1^2\} |u|_{1,2,\Omega} |v|_{1,2,\Omega}
\end{aligned}
$$

where $\Lambda > 0$ is the largest eigenvalue of $[A_{ij}]_{1 \le i,j \le 2}$, $M_1 = \max\{\Lambda, \beta, \|C\|_{\infty,\Omega}\}$, and K_1 is the constant given by Poincaré's inequality, which depends only on Ω. That is,

$$
a(u,v) \le M |u|_{1,2,\Omega} |v|_{1,2,\Omega}. \tag{52}
$$

for another positive constant M. By definition of weak solution, we know that for all $v \in H_0^1(\Omega)$, $a(u,v) = \langle f, v \rangle$, and for all $v \in \mathscr{S}_d$, $a(u_S, v) = \langle f, v \rangle$. Since $\mathscr{S}_d \subset H_0^1(\Omega)$, we can say that for all $v \in \mathscr{S}_d$,

$$
a(u - u_S, v) = 0, \quad \forall v \in \mathscr{S}_d. \tag{53}
$$

Now, define $u_{best} := \arg\min_{s \in \mathscr{S}_d} |u - s|_{1,2,\Omega}$. Then, we have

$$
\begin{aligned}
\mu |u_{best} - u_S|_{1,2,\Omega}^2 &\le a(u_{best} - u_S, u_{best} - u_S) \\
&= a(u_{best} - u, u_{best} - u_S) \\
&\le M |u_{best} - u|_{1,2,\Omega} \, |u_{best} - u_S|_{1,2,\Omega} \\
\Rightarrow \mu |u_{best} - u_S|_{1,2,\Omega} &\le M |u_{best} - u|_{1,2,\Omega} \\
\mu |u - u_S|_{1,2,\Omega} &\le \mu |u - u_{best}|_{1,2,\Omega} + \mu |u_{best} - u_S|_{1,2,\Omega} \\
&\le \mu |u - u_{best}|_{1,2,\Omega} + M |u_{best} - u|_{1,2,\Omega} \\
\Rightarrow \qquad |u - u_S|_{1,2,\Omega} &\le \frac{\mu + M}{\mu} |u - u_{best}|_{1,2,\Omega} \le \frac{\mu + M}{\mu} C |u|_{d+1,2,\Omega} |\Delta|^d.
\end{aligned}
$$

These complete the proof.

We next explain the convergence in L_2 norm. When Ω is a convex domain, the convergence rate $||u - u_{best}||_{L_2(\Omega)}$ should be optimal based on a generalization of the well-known Aubin–Nitsche technique (cf. [8]) for Poisson equation. That is, we have

Theorem 8 *Suppose that the conditions of Theorem 7 are satisfied, and further suppose that the underlying Lipschitz domain Ω is convex. Let u_S be the weak solution of (1). Then for $d \ge 1$,*

$$
\|u - u_S\|_{L_2(\Omega)} \le C |\Delta|^{d+1} |u|_{d+1,2,\Omega} \tag{54}
$$

for a positive constant C independent of u.

Proof For $u - u_S \in L_2(\Omega)$, we can find the weak solution $w \in H_0^1(\Omega)$ satisfying

$$a(v, w) = \langle u - u_S, v \rangle, \quad \forall v \in H_0^1(\Omega). \tag{55}$$

Indeed, let $\hat{a}(u, v) = a(v, u)$ be a new bilinear form. By using the same proof of Theorem 3, we can show $\hat{a}(u, v)$ is a bounded bilinear form and $\hat{a}(u, u)$ is coercive since $\hat{a}(u, u) = a(u, u)$. By the Lax–Milgram theorem, there exists a weak solution w satisfying (55). It is known that $w \in H^2(\Omega)$ when Ω is convex (cf. [13]) and satisfies $|w|_{2,2,\Omega} \leq C\|u - u_S\|_{L^2(\Omega)}$ for a positive constant $C > 0$ independent of u and u_S.

Thus, we use (53) with an appropriate $v \in \mathscr{S}_d$,

$$\begin{aligned}
\|u - u_S\|_{L_2(\Omega)}^2 &= \langle u - u_S, u - u_S \rangle = a(u - u_S, w) \\
&= a(u - S, w - v) \leq M|u - u_S|_{1,2,\Omega}\ |w - v|_{1,2,\Omega} \\
&\leq MC|\Delta|^d |u|_{d+1,2,\Omega} C|\Delta||w|_{2,2,\Omega} \\
&\leq MC|\Delta|^{d+1} |u|_{d+1,2,\Omega} C\|u - u_S\|_{L_2(\Omega)},
\end{aligned}$$

for positive constants C which are different in different lines. It now follows that

$$\|u - u_S\|_{L_2(\Omega)} \leq C|\Delta|^{d+1}|u|_{d+1,2,\Omega}$$

for another positive constant C. This completes the proof.

4 Numerical Results

4.1 Description of Our Implementation

In this section, we explain our implementation to numerically solve general second-order elliptic PDEs. It is an adaptation of the method detailed in [12] which uses polygonal splines to solve Poisson equations, which is in turn based on the method in [1], which details how to solve both linear and nonlinear PDEs with multivariate splines.

Our goal will be to solve for a vector of coefficients $\mathbf{u}$. We can begin in the same place as in [12], first constructing a matrix H to determine continuity conditions. If two polygons share an edge, then there are $d + 1$ pairs of elements supported on that edge between the two polygons, and each pair share values on the edge. Hence we force their respective coefficients to match, resulting in a linear system summarized by $H\mathbf{u} = 0$. We can similarly represent our boundary conditions by a linear system $B\mathbf{u} = \mathbf{g}$.

An important difference arises from here: We will need to form a different "stiffness" matrix than in the simpler Poisson case. In particular, in $\mathbb{R}^D$, using degree d polygonal splines, the new left-hand side of the weak form of the problem can be simplified to the following:

$$\sum_{P_n\in\Delta}\sum_{k=1}^{dn} u_k\left[\sum_{i,j=1}^{D}\int_{P_n} A_{ij}\frac{\partial v}{\partial x_i}\frac{\partial L_k}{\partial x_j}+\int_{P_n} cvL_k\right]$$

where we have expressed $u\approx u_S=\sum_{k=1}^{dn} u_kL_k$ for some coefficients u_k where L_k is an ordering of the interpolatory basis of $\mathscr{S}_d(\Delta)$ (which, when restricted to the domain P_n, is simply $\Psi_d(P_n)$). Similarly, write $f\approx f_S=\sum_{k=1}^{dn} f_kL_k$ and notice that the right-hand side of the weak form will be equal to $\sum_{P_n\in\Delta}\sum_{k=1}^{dn} f_k\int_{P_n} vL_k$ for any $v\in\mathscr{S}_d(\Delta)\cap H_0^1(\Omega)$. Hence, it must be true for $v=L_m$ for $m=1,2,...,dn$. We can thus construct the following matrices:

$$M=[M_{P_n}]_{P_n\in\Delta} \text{ where } M_{P_n}=\left(M_{P_n,p,q}\right)_{p,q=1}^{D}, \text{ and } M_{P_n,p,q}=\int_{P_n} L_pL_q\ ;$$

$$\mathscr{K}=[\mathscr{K}_{P_n}]_{P_n\in\Delta} \text{ where } \mathscr{K}_{P_n}=\sum_{i,j=1}^{D}\mathscr{K}_{P_n}^{i,j} \text{ and}$$

$$\mathscr{K}_{P_n}^{i,j}=\left(\mathscr{K}_{P_n,p,q}^{i,j}\right)_{p,q=1}^{D} \text{ where } \mathscr{K}_{P_n,p,q}^{i,j}=\int_{P_n} A_{ij}\frac{\partial L_p}{\partial x_i}\frac{\partial L_q}{\partial x_j}\ ;$$

$$\mathscr{M}_{P_n}=\left(\mathscr{M}_{P_n,p,q}\right)_{p,q=1}^{D} \text{ where } \mathscr{M}_{P_n,p,q}=\int_{P_n} CL_pL_q\ ;$$

$$K=[\mathscr{K}_{P_n}]_{P_n\in\Delta}+[\mathscr{M}_{P_n}]_{P_n\in\Delta};\quad \mathbf{u}=(u_k)_{k=1}^{D}\ ;\quad \mathbf{f}=(f_k)_{k=1}^{D}\ ;$$

where the integrals are computed by first decomposing each polygon into quadrilaterals, and then using the tensor product of the Gauss quadrature formula of high order, say order 5×5, on each quadrilateral.

Then, notice that we can rewrite our weak formulation as

$$K\mathbf{u}=M\mathbf{f}.$$

Our minimization in (24) can be recast in terms of polygonal splines as

$$\min_{\substack{\mathbf{u}\\ H\mathbf{u}=0,B\mathbf{u}=\mathbf{g}}}\frac{1}{2}\mathbf{u}^TK\mathbf{u}-\mathbf{f}^TM\mathbf{u}$$

which is a constrained minimization problem which can be solved using the well-known iterative method described in [1]. We have implemented the computational scheme in MATLAB and experimented with many second-order elliptic PDEs. Some numerical results will be shown in the next section. Some of these results also involve first derivatives; these are implemented as another stiffness matrix added to K: First,

we define

$$\mathscr{J}_{P_n} = \sum_{k=1}^{2} \mathscr{J}_{P_n}^k$$

where $\mathscr{J}_{P_n}^k = \left(\mathscr{J}_{P_n,p,q}^k\right)_{p,q=1}^{D}$ and $\mathscr{J}_{P_n,p,q}^k = \int_{P_n} B_k L_p \frac{\partial L_q}{\partial x_k}$ where B_k is the appropriate coefficient function. Then, we instead use $K = [\mathscr{K}_{P_n}]_{P_n\in\Delta} + [\mathscr{J}_{P_n}]_{P_n\in\Delta} + [\mathscr{M}_{P_n}]_{P_n\in\Delta}$.

It is worth mentioning that other finite element methods accommodate continuity conditions directly rather than solving a linear system, which saves computational power and time. However, our approach is designed conveniently to implement more complex continuity conditions; see Example 7.

4.2 Numerical Results of Elliptic PDEs

This section is divided into two parts. In the first part, we demonstrate the power of polygonal splines as a tool for numerically solving some general second-order elliptic PDEs. In the second part, we show the potential to use these numerical solutions to approximate the solutions of parabolic equations and hyperbolic equations. In all the following examples, we denote by u_S the spline solution, and by u the exact solution. To approximate the L^2 error, we report the root-mean-squared (RMS) error $E_{RMS} = ||u - u_S||_{RMS}$ of the spline solution based on 1001×1001 equally spaced points over Ω. Since $\nabla(u - u_S) = \left(\frac{\partial}{\partial x}(u - u_S), \frac{\partial}{\partial y}(u - u_S)\right)$, we report the RMS error $\nabla E_{RMS} = ||\nabla(u - u_S)||_{RMS}$, which is the average of the RMS error of $\frac{\partial}{\partial x}(u - u_S)$ and $\frac{\partial}{\partial y}(u - u_S)$. We also report the mesh size (i.e., the longest edge length) of the partition at each iteration and the computed rate of convergence in reference to the mesh size—in light of Theorems 7 and 8, we expect the rates to be 4 for degree 3 in the L^2 norm, 3 for degree 2 in the L^2 norm and degree 3 in the H^1 norm, and 2 for degree 2 in the H^1 norm.

Let us begin with numerical solutions of some standard second-order elliptic PDEs.

Example 2 We return to Example 3 on the unit square $\Omega = (0, 1) \times (0, 1)$ to demonstrate convergence of the method. We will set $\varepsilon = 10^{-5}$ and choose f and g so that

$$u(x, y) = \frac{(1 + x)^2}{4} \sin(2\pi xy) \tag{56}$$

is the exact solution. We use the following polygonal partition shown in Fig. 3.

We employ our polygonal spline method to solve (1) with exact solution in (56). Our numerical results are shown below in Tables 1 and 2.

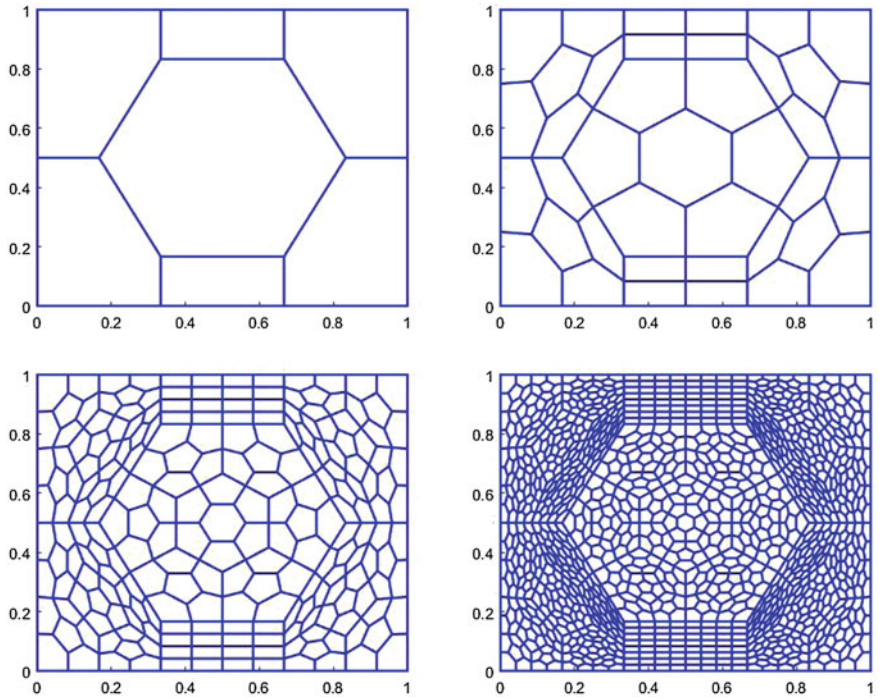

Fig. 3 A partition of the unit square and a few refinements

Table 1 Degree-2 polygonal spline approximation of solution to Example 2 with exact solution in (56)

# P	Mesh	E_{RMS}	Rate	∇E_{RMS}	Rate
39	2.50e-01	5.47e-03	0.00	1.34e-01	0.00
219	1.25e-01	4.16e-04	3.72	2.60e-02	2.36
1251	6.25e-02	3.68e-05	3.50	5.17e-03	2.33
7251	3.13e-02	3.29e-06	3.48	1.03e-03	2.33

Table 2 Degree-3 polygonal spline approximation of solution to Example 2 with exact solution in (56)

# P	Mesh	E_{RMS}	Rate	∇E_{RMS}	Rate
39	2.50e-01	9.01e-04	0.00	1.61e-02	0.00
219	1.25e-01	2.74e-05	5.04	1.41e-03	3.52
1251	6.25e-02	1.25e-06	4.45	1.31e-04	3.43
7251	3.13e-02	6.92e-08	4.18	1.22e-05	3.43

Table 3 Degree-2 bivariate spline approximation of solution to Example 2 with exact solution in (56)

# T	Mesh	E_{RMS}	Rate	∇E_{RMS}	Rate
40	3.54e-01	6.94e-03	0.00	2.09e-01	0.00
160	1.77e-01	8.29e-04	3.06	5.38e-02	1.96
640	8.84e-02	1.00e-04	3.05	1.34e-02	2.00
2560	4.42e-02	1.22e-05	3.03	3.32e-03	2.01

Table 4 Degree-3 bivariate spline approximation of solution to Example 2 with exact solution in (56)

# T	Mesh	E_{RMS}	Rate	∇E_{RMS}	Rate
40	3.54e-01	7.16e-04	0.00	3.15e-02	0.00
160	1.77e-01	4.43e-05	4.01	3.96e-03	2.99
640	8.84e-02	5.33e-06	3.06	4.96e-04	3.00
2560	4.42e-02	5.52e-06	–0.05	7.22e-05	2.78

Table 5 Polygonal splines' degrees of freedom

# P	DoF ($d = 2$)	DoF ($d = 3$)
39	179	313
219	886	1657
1251	4958	9313
7251	28654	53857

The numerical results in Tables 1 and 2 show that the polygonal spline method works very well. We shall compare with the solution using degree-2 and degree-3 bivariate splines triangulation of the same domain. We chose a grid-based initial triangulation with close to the same number of elements as our initial polygonal partition.

From Tables 1, 2, 3, and 4, we can see that polygonal splines can produce a more accurate solution on polygonal partitions containing a similar number of polygons as a triangulation of the same domain.

It is worth noting the difference in degrees of freedom in this example. In particular, the polygonal splines have significantly more degrees of freedom than each iteration of triangular spline. However, this does not seem representative in general—for example, one could imagine removing edges from a triangulation to form a polygonal partition of the same domain while reducing the number of degrees of freedom. Regardless, there is no doubt that our polygonal spline methods are more numerically taxing than traditional bivariate spline methods. At each iteration, we have the following numbers of degrees of freedom (Tables 5 and 6).

As we will use the same partitions for each example in this paper, the reader can refer back to these tables.

Table 6 Bivariate splines' degrees of freedom

# T	DoF ($d = 2$)	DoF ($d = 3$)
40	97	205
160	353	769
640	1345	2977
2560	5249	11713

Table 7 Degree-2 polygonal spline approximation of solution to Example 3 with exact solution (58)

# P	Mesh	E_{RMS}	Rate	∇E_{RMS}	Rate
39	2.50e-01	1.30e-04	0.00	3.82e-03	0.00
219	1.25e-01	1.08e-05	3.59	7.47e-04	2.35
1251	6.25e-02	1.09e-06	3.30	1.54e-04	2.28
7251	3.13e-02	1.57e-07	2.80	3.40e-05	2.18

Example 3 Here is another example of an elliptic second-order PDE: Let

$$\begin{bmatrix} A_{11} & A_{12} \\ A_{21} & A_{22} \end{bmatrix} = \begin{bmatrix} 1+\varepsilon & 1 \\ 1 & 1+\varepsilon \end{bmatrix}$$

for some $\varepsilon > 0$, and let $C = 1$, and solve the PDE given by

$$-\sum_{i,j=1}^{2} \frac{\partial}{\partial x_j}\left(A_{ij}\frac{\partial u}{\partial x_i}\right) + \frac{\partial u}{\partial x_1} + \frac{\partial u}{\partial x_2} + Cu = f \text{ in } \Omega; \quad u = g \text{ on } \partial\Omega. \tag{57}$$

To test our method, we shall choose f and g so that

$$u = (1 + x^2 + y^2)^{-1} \tag{58}$$

is the exact solution.

According to Corollary 1, this elliptic PDE has a unique weak solution. Although this PDE technically does not fit with our computational scheme in the previous section because the PDE involves the first-order derivatives, our minimization scheme (24) with additional first-order derivative terms still produces good results. In fact, we can even use $\varepsilon = 0$, which makes this PDE nonelliptic, and still produce good solutions. We use the same partition as in Example 2 to solve this PDE. Tables 7 and 8 show the results of our minimization, using the nonelliptic condition $\varepsilon = 0$.

Similarly, the minimization (24) with first-order derivatives based on bivariate splines can also produce good numerical results. For comparison, Tables 9 and 10 tabulate the results of the same computation using bivariate splines of degree 2 and degree 3 over grid-based right triangulations of the same domain.

Table 8 Degree-3 polygonal spline approximation of solution to Example 3 with exact solution (58)

# P	Mesh	E_{RMS}	Rate	∇E_{RMS}	Rate
39	2.50e-01	7.64e-06	0.00	2.41e-04	0.00
219	1.25e-01	3.70e-07	4.37	2.41e-05	3.32
1251	6.25e-02	1.99e-08	4.21	2.36e-06	3.35
7251	3.13e-02	1.25e-09	4.00	2.41e-07	3.29

Table 9 Degree-2 bivariate spline approximation of solution to Example 3 with exact solution in (58)

# T	Mesh	E_{RMS}	Rate	∇E_{RMS}	Rate
40	3.54e-01	4.80e-04	0.00	1.14e-02	0.00
160	1.77e-01	5.23e-05	3.20	2.70e-03	2.07
640	8.84e-02	6.21e-06	3.07	7.14e-04	1.92
2560	4.42e-02	8.53e-07	2.86	2.29e-04	1.64

Table 10 Degree-3 bivariate spline approximation of solution to Example 3 with exact solution in (58)

# T	Mesh	E_{RMS}	Rate	∇E_{RMS}	Rate
40	3.54e-01	2.43e-05	0.00	9.87e-04	0.00
160	1.77e-01	1.81e-06	3.75	1.44e-04	2.77
640	8.84e-02	1.29e-07	3.81	2.01e-05	2.84
2560	4.42e-02	9.69e-09	3.74	2.97e-06	2.76

4.3 Numerical Solutions of Parabolic and Hyperbolic PDEs

Example 4 We return again to Example (3) on the unit square $\Omega = (0, 1) \times (0, 1)$, but this time with $\varepsilon = 0$. We will choose f and g so that

$$u(x, y) = \frac{(1 + x)^2}{4} \sin(2\pi xy) \tag{59}$$

is the exact solution. Notice that, in this case, the PDE is not elliptic. However, our method still approximates the true solution quite well. We will show the convergence of our approximations for decreasing values of ε.

For comparison, let us show the results of the same PDE using bivariate splines over a triangulation of the same domain instead (Tables 11, 12, 13, 14, 15, 16, 17, 18, 19, 20, 21, and 22).

The numerical results in the tables above show that the polygonal spline method is efficient in approximating the solutions of nonelliptic PDEs.

Table 11 Degree-2 polygonal spline approximation of solution to Example 4 with exact solution in (59) and $\varepsilon = 10^{-3}$

# P	Mesh	E_{RMS}	Rate	∇E_{RMS}	Rate
39	2.50e-01	5.27e-03	0.00	1.33e-01	0.00
219	1.25e-01	6.41e-04	3.04	2.61e-02	2.35
1251	6.25e-02	5.54e-04	0.21	6.14e-03	2.09
7251	3.13e-02	5.56e-04	–0.00	3.71e-03	0.73

Table 12 Degree-3 polygonal spline approximation of solution to Example 4 with exact solution in (59) and $\varepsilon = 10^{-3}$

# P	Mesh	E_{RMS}	Rate	∇E_{RMS}	Rate
39	2.50e-01	1.39e-03	0.00	1.71e-02	0.00
219	1.25e-01	5.71e-04	1.29	3.70e-03	2.21
1251	6.25e-02	5.56e-04	0.04	3.55e-03	0.06
7251	3.13e-02	5.56e-04	–0.00	3.65e-03	–0.04

Table 13 Degree-2 polygonal spline approximation of solution to Example 4 with exact solution in (59) and $\varepsilon = 10^{-5}$

# P	Mesh	E_{RMS}	Rate	∇E_{RMS}	Rate
39	2.50e-01	5.47e-03	0.00	1.34e-01	0.00
219	1.25e-01	4.15e-04	3.72	2.60e-02	2.36
1251	6.25e-02	3.69e-05	3.49	5.17e-03	2.33
7251	3.13e-02	6.45e-06	2.52	1.03e-03	2.33

Table 14 Degree-3 polygonal spline approximation of solution to Example 4 with exact solution in (59) and $\varepsilon = 10^{-5}$

# P	Mesh	E_{RMS}	Rate	∇E_{RMS}	Rate
39	2.50e-01	9.06e-04	0.00	1.61e-02	0.00
219	1.25e-01	3.11e-05	4.86	1.41e-03	3.52
1251	6.25e-02	6.10e-06	2.35	1.37e-04	3.37
7251	3.13e-02	5.62e-06	0.12	4.29e-05	1.67

Table 15 Degree-2 polygonal spline approximation of solution to Example 4 with exact solution in (59) and $\varepsilon = 10^{-10}$

# P	Mesh	E_{RMS}	Rate	∇E_{RMS}	Rate
39	2.50e-01	5.47e-03	0.00	1.34e-01	0.00
219	1.25e-01	4.16e-04	3.72	2.60e-02	2.36
1251	6.25e-02	3.68e-05	3.50	5.17e-03	2.33
7251	3.13e-02	3.29e-06	3.48	1.03e-03	2.33

Table 16 Degree-3 polygonal spline approximation of solution to Example 4 with exact solution in (59) and $\varepsilon = 10^{-10}$

# P	Mesh	E_{RMS}	Rate	∇E_{RMS}	Rate
39	2.50e-01	9.01e-04	0.00	1.61e-02	0.00
219	1.25e-01	2.74e-05	5.04	1.41e-03	3.52
1251	6.25e-02	1.25e-06	4.45	1.31e-04	3.43
7251	3.13e-02	6.92e-08	4.18	1.22e-05	3.43

Table 17 Degree-2 bivariate spline approximation of solution to Example 4 with exact solution in (59) and $\varepsilon = 10^{-3}$

# T	Mesh	E_{RMS}	Rate	∇E_{RMS}	Rate
40	3.54e-01	6.91e-03	0.00	2.09e-01	0.00
160	1.77e-01	9.63e-04	2.84	5.38e-02	1.96
640	8.84e-02	5.55e-04	0.80	1.37e-02	1.97
2560	4.42e-02	5.53e-04	0.00	4.68e-03	1.55

Table 18 Degree-3 bivariate spline approximation of solution to Example 4 with exact solution in (59) and $\varepsilon = 10^{-3}$

# T	Mesh	E_{RMS}	Rate	∇E_{RMS}	Rate
40	3.54e-01	7.40e-04	0.00	3.14e-02	0.00
160	1.77e-01	5.37e-04	0.46	4.99e-03	2.66
640	8.84e-02	5.52e-04	–0.04	3.36e-03	0.57
2560	4.42e-02	5.55e-04	–0.01	3.60e-03	–0.10

Table 19 Degree-2 bivariate spline approximation of solution to Example 4 with exact solution in (59) and $\varepsilon = 10^{-5}$

# T	Mesh	E_{RMS}	Rate	∇E_{RMS}	Rate
40	3.54e-01	6.94e-03	0.00	2.09e-01	0.00
160	1.77e-01	8.29e-04	3.06	5.38e-02	1.96
640	8.84e-02	1.00e-04	3.05	1.34e-02	2.00
2560	4.42e-02	1.32e-05	2.92	3.32e-03	2.01

Table 20 Degree-3 bivariate spline approximation of solution to Example 4 with exact solution in (59) and $\varepsilon = 10^{-5}$

# T	Mesh	E_{RMS}	Rate	∇E_{RMS}	Rate
40	3.54e-01	7.16e-04	0.00	3.15e-02	0.00
160	1.77e-01	4.43e-05	4.01	3.96e-03	2.99
640	8.84e-02	5.33e-06	3.06	4.96e-04	3.00
2560	4.42e-02	5.52e-06	–0.05	7.22e-05	2.78

Table 21 Degree-2 bivariate spline approximation of solution to Example 4 with exact solution in (59) and $\varepsilon = 10^{-10}$

# T	Mesh	E_{RMS}	Rate	∇E_{RMS}	Rate
40	3.54e-01	6.94e-03	0.00	2.09e-01	0.00
160	1.77e-01	8.29e-04	3.06	5.38e-02	1.96
640	8.84e-02	1.00e-04	3.05	1.34e-02	2.00
2560	4.42e-02	1.22e-05	3.03	3.32e-03	2.01

Table 22 Degree-3 bivariate spline approximation of solution to Example 4 with exact solution in (59) and $\varepsilon = 10^{-10}$

# T	Mesh	E_{RMS}	Rate	∇E_{RMS}	Rate
40	3.54e-01	7.18e-04	0.00	3.15e-02	0.00
160	1.77e-01	4.59e-05	3.97	3.96e-03	2.99
640	8.84e-02	2.93e-06	3.97	4.95e-04	3.00
2560	4.42e-02	1.85e-07	3.98	6.19e-05	3.00

Table 23 Weak Galerkin approximation of solution to Example 5

# Poly's	Mesh	$\|\|u - u_{WG}\|\|_{L^2}$	Rate	$\|\|\nabla u - \nabla u_{WG}\|\|_{H^1}$	Rate
64	1.25e-01	1.46e-03	0.00	2.52e-02	0.00
256	6.25e-02	3.74e-04	1.96	1.23e-02	9.98e-01
1024	3.13e-02	9.47e-05	1.98	6.31e-03	9.98e-01
4096	1.56e-02	2.39e-05	1.99	3.16e-03	9.98e-01

Example 5 Let

$$\begin{bmatrix} A_{11} & A_{12} \\ A_{21} & A_{22} \end{bmatrix} = \begin{bmatrix} xy & 0 \\ 0 & xy \end{bmatrix}$$

and $C = 0$. Choose f and g so that

$$u = x(1-x)y(1-y) \tag{60}$$

is the exact solution. This was studied in [19]. As in Example 4, this is a "nearly elliptic" PDE, but with some degeneracy at the origin. We shall use a different partition of the unit square this time, simply using a uniform grid of squares, as was the case in the original paper [19]. The weak Galerkin method presented in this paper retrieved the results shown in Table 23.

We use our method with polygonal splines to solve the PDE above and find that our method can produce much better results.

Comparison of Tables 23, 24, and 25 shows that our polygonal spline method produces a much more accurate solution. These results call for some remarks. First,

Table 24 Degree-2 polygonal spline approximation of solution to Example 5

# P	Mesh	E_{RMS}	Rate	∇E_{RMS}	Rate
64	1.25e-01	1.83e-06	0.00	1.39e-04	0.00
256	6.25e-02	9.85e-08	4.22	1.60e-05	3.12
1024	3.13e-02	5.65e-09	4.12	1.91e-06	3.07
4096	1.56e-02	3.42e-10	4.05	2.33e-07	3.04

Table 25 Degree-3 polygonal spline approximation of solution to Example 5

# P	Mesh	E_{RMS}	Rate	∇E_{RMS}	Rate
64	2.50e-01	3.59e-12	0.00	5.63e-11	0.00
256	1.25e-01	1.40e-11	–1.96	2.07e-10	–1.88
1024	6.25e-02	2.34e-11	–0.74	2.71e-10	–0.39
4096	3.13e-02	4.47e-11	–0.93	5.61e-10	–1.05

Table 26 Degree-2 polygonal spline approximation of solution to Example 5 over nongrid partition

# P	Mesh	E_{RMS}	Rate	∇E_{RMS}	Rate
39	2.50e-01	3.66e-05	0.00	1.19e-03	0.00
219	1.25e-01	3.09e-06	3.57	2.29e-04	2.38
1251	6.25e-02	2.75e-07	3.49	4.59e-05	2.32

Table 27 Degree-3 polygonal spline approximation of solution to Example 5 over nongrid partition

# P	Mesh	E_{RMS}	Rate	∇E_{RMS}	Rate
39	2.50e-01	3.10e-06	0.00	9.17e-05	0.00
219	1.25e-01	1.22e-07	4.66	7.07e-06	3.70
1251	6.25e-02	4.59e-09	4.74	5.96e-07	3.57

it is worth pointing out that our MATLAB code can only achieve $1e-11$ accuracy. In Table 25, the rates of convergence become negative due to round-off errors. That is, polygonal splines of degree-3 converged to the solution *virtually instantly*. Some improved performance has been observed before when the solution is a polynomial, but we would not normally expect immediate retrieval of the solution of a degree-4 polynomial using only degree-3 splines. The degree-2 splines also appear to have an increased order of convergence $O(h^4)$. We are interested in why the performance has been increased here, and our investigation seems to show that the partition plays a role. If we run a few iterations to solve the same problem over the unit square based on the partition from Example 2, we retrieve the following results shown in Tables 26 and 27.

Table 28 Degree-2 polygonal spline approximation of solution to Example 6 with $\varepsilon = 10^{-3}$

# P	Mesh	E_{RMS}	Rate	∇E_{RMS}	Rate
39	2.50e-01	1.28e-03	0.00	5.58e-02	0.00
219	1.25e-01	4.22e-04	1.60	2.38e-02	1.23
1251	6.25e-02	4.04e-04	0.07	2.28e-02	0.06
7251	3.13e-02	3.99e-04	0.02	2.15e-02	0.09

Table 29 Degree-3 polygonal spline approximation of solution to Example 6 with $\varepsilon = 10^{-3}$

# P	Mesh	E_{RMS}	Rate	∇E_{RMS}	Rate
39	2.50e-01	4.62e-04	0.00	2.02e-02	0.00
219	1.25e-01	4.07e-04	0.18	2.24e-02	–0.15
1251	6.25e-02	4.00e-04	0.02	2.18e-02	0.04
7251	3.13e-02	3.99e-04	0.01	1.81e-02	0.26

Table 30 Degree-2 polygonal spline approximation of solution to Example 6 with $\varepsilon = 10^{-5}$

# P	Mesh	E_{RMS}	Rate	∇E_{RMS}	Rate
39	2.50e-01	1.83e-03	0.00	7.70e-02	0.00
219	1.25e-01	2.97e-04	2.62	3.03e-02	1.35
1251	6.25e-02	4.51e-05	2.72	1.25e-02	1.28
7251	3.13e-02	6.32e-06	2.84	3.67e-03	1.77

We can see that this time the numerical solutions are closer to the expected rate of convergence. Thus, the grid partition plays a role to the solution of this problem. We would like to invite the interested reader to investigate it further.

Example 6 Consider the following example:

$$-\varepsilon\Delta u + (2-y^2)D_x u + (2-x)D_y u + (1+(1+x)(1+y)^2)u = f, (x,y) \in \Omega \tag{61}$$

with $\Omega = (0,1)^2$, and $u|_{\partial\Omega} = g$. The function f is so chosen that the exact solution is

$$u(x,y) = 1 + \sin(\pi(1+x)(1+y)^2/8).$$

When $\varepsilon = 0$, this is a hyperbolic test problem considered in [5, 14, 15]. However, for positive values of ε, this is an elliptic PDE. We can well approximate a solution to the hyperbolic problem by using very small positive values of ε.

For comparison, here are the results of the same computation using bivariate splines over a triangulation of the same domain (Tables 28, 29, 30, 31, 32, 33, 34, 35, 36, 37, 38, 39, and 40).

Table 31 Degree-3 polygonal spline approximation of solution to Example 6 with $\varepsilon = 10^{-5}$

# P	Mesh	E_{RMS}	Rate	∇E_{RMS}	Rate
39	2.50e-01	3.71e-05	0.00	2.50e-03	0.00
219	1.25e-01	6.66e-06	2.48	8.58e-04	1.54
1251	6.25e-02	5.19e-06	0.36	1.42e-03	–0.72
7251	3.13e-02	4.36e-06	0.25	2.02e-03	–0.51

Table 32 Degree-2 polygonal spline approximation of solution to Example 6 with $\varepsilon = 10^{-10}$

# P	Mesh	E_{RMS}	Rate	∇E_{RMS}	Rate
39	2.50e-01	1.84e-03	0.00	7.73e-02	0.00
219	1.25e-01	3.05e-04	2.59	3.10e-02	1.32
1251	6.25e-02	5.26e-05	2.54	1.43e-02	1.12
7251	3.13e-02	8.46e-06	2.63	5.60e-03	1.35

Table 33 Degree-3 polygonal spline approximation of solution to Example 6 with $\varepsilon = 10^{-10}$

# P	Mesh	E_{RMS}	Rate	∇E_{RMS}	Rate
39	2.50e-01	3.49e-05	0.00	2.37e-03	0.00
219	1.25e-01	2.00e-06	4.13	3.46e-04	2.78
1251	6.25e-02	1.24e-07	4.01	5.26e-05	2.72
7251	3.13e-02	1.84e-08	2.75	1.88e-05	1.49

Table 34 Degree-2 bivariate spline approximation of solution to Example 6 with $\varepsilon = 10^{-3}$

# T	Mesh	E_{RMS}	Rate	∇E_{RMS}	Rate
40	3.54e-01	1.52e-04	0.00	4.07e-03	0.00
160	1.77e-01	4.58e-05	1.73	1.70e-03	1.26
640	8.84e-02	2.87e-05	0.67	1.13e-03	0.58
2560	4.42e-02	2.67e-05	0.10	1.13e-03	–0.00

Table 35 Degree-3 bivariate spline approximation of solution to Example 6 with $\varepsilon = 10^{-3}$

# T	Mesh	E_{RMS}	Rate	∇E_{RMS}	Rate
40	3.54e-01	3.08e-05	0.00	7.95e-04	0.00
160	1.77e-01	2.82e-05	0.13	1.03e-03	–0.37
640	8.84e-02	2.69e-05	0.07	1.13e-03	–0.13
2560	4.42e-02	2.66e-05	0.02	1.21e-03	–0.10

Table 36 Degree-2 bivariate spline approximation of solution to Example 6 with $\varepsilon = 10^{-5}$

# T	Mesh	E_{RMS}	Rate	∇E_{RMS}	Rate
40	3.54e-01	1.58e-04	0.00	4.64e-03	0.00
160	1.77e-01	3.93e-05	2.01	2.21e-03	1.07
640	8.84e-02	9.81e-06	2.00	1.08e-03	1.04
2560	4.42e-02	2.40e-06	2.03	5.04e-04	1.09

Table 37 Degree-3 bivariate spline approximation of solution to Example 6 with $\varepsilon = 10^{-5}$

# T	Mesh	E_{RMS}	Rate	∇E_{RMS}	Rate
40	3.54e-01	5.36e-06	0.00	2.65e-04	0.00
160	1.77e-01	6.10e-07	3.13	5.66e-05	2.23
640	8.84e-02	3.13e-07	0.96	3.86e-05	0.55
2560	4.42e-02	2.99e-07	0.07	6.72e-05	–0.80

Table 38 Degree-2 bivariate spline approximation of solution to Example 6 with $\varepsilon = 10^{-10}$

# T	Mesh	E_{RMS}	Rate	∇E_{RMS}	Rate
40	3.54e-01	1.58e-04	0.00	4.65e-03	0.00
160	1.77e-01	3.94e-05	2.01	2.22e-03	1.06
640	8.84e-02	9.90e-06	1.99	1.10e-03	1.01
2560	4.42e-02	2.46e-06	2.01	5.48e-04	1.01

Table 39 Degree-3 bivariate spline approximation of solution to Example 6 with $\varepsilon = 10^{-10}$

# T	Mesh	E_{RMS}	Rate	∇E_{RMS}	Rate
40	3.54e-01	5.43e-06	0.00	2.67e-04	0.00
160	1.77e-01	5.68e-07	3.26	5.57e-05	2.26
640	8.84e-02	6.93e-08	3.03	1.42e-05	1.97
2560	4.42e-02	8.55e-09	3.02	3.40e-06	2.06

We can see that the polygonal spline solutions approximate the exact solution very well. However, as in (59), we see that this PDE has a unique weak solution but does not satisfy the assumptions of Theorem 5. Nevertheless, our method works well as shown in Tables 36 and 37.

Example 7 For another example, the following problem is parabolic for $y > 0$ and hyperbolic for $y \leq 0$:

$$\begin{aligned} -\varepsilon D_{yy}u + D_x u + c_1 u = 0, \quad (x, y) \in (-1, 1) \times (0, 1) \\ D_x u + c_2 u = 0, \quad (x, y) \in (-1, 1) \times (-1, 0] \end{aligned} \tag{62}$$

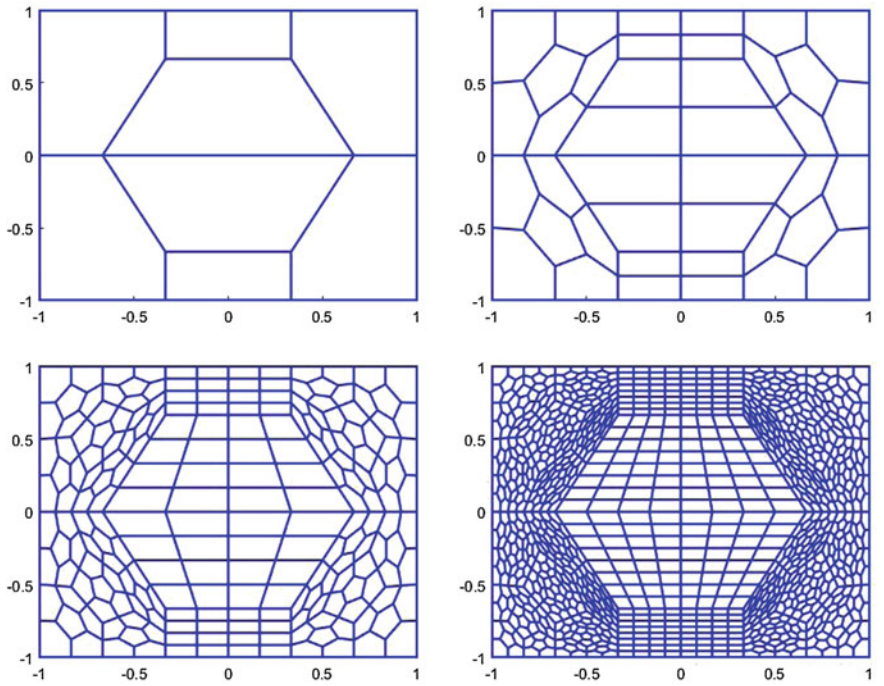

Fig. 4 A partition of $\Omega = [-1, 1]^2$ and a few refinements

with $u|_{\partial\Omega} = g$, for any constants $c_1 > 0$ and $c_2 > 0$. This PDE was studied in [15]. Note that the solution is discontinuous at $y = 0$. We can solve the following general elliptic PDE to estimate the solution to this problem:

$$\begin{aligned} -\eta D_{xx}u - \varepsilon D_{yy}u + D_x u + c_1 u = 0, \quad (x, y) \in (-1, 1) \times (0, 1) \\ -\eta \Delta u + D_x u + c_2 u = 0, \quad (x, y) \in (-1, 1) \times (-1, 0] \end{aligned} \tag{63}$$

with $u|_{\partial\Omega} = g$ and $\eta > 0$. We can approximate the solution to (62) by letting $\eta > 0$ go to zero and use spline functions which are not necessarily continuous at $y = 0$. Let the exact solution, $u(x, y)$, of (62) be the following piecewise function:

$$\begin{array}{ll} \sin(\pi(1 + y)/2) \exp(-(c_1 + \varepsilon\pi^2/4)(1 + x)), & -1 \le x \le 1, 0 \le y \le 1 \\ \sin(\pi(1 + y)/2) \exp(-c_2(1 + x)), & -1 \le x \le 1, -1 < y \le 0. \end{array} \tag{64}$$

We set $\varepsilon = 0.05$ and use a similar partition to the one from Example 2, scaled to cover the domain $\Omega = [-1, 1]^2$ and with an added edge to account for the discontinuity at $y = 0$. See Fig. 4

Table 40 Degree-2 polygonal spline approximation of solution to (62) with exact solution (64) when $\eta = 10^{-10}$, $c_1 = c_2 = 0.1$

# P	Mesh	E_{RMS}	Rate	∇E_{RMS}	Rate
40	6.67e-01	6.80e-03	0.00	2.13e-01	0.00
208	3.33e-01	2.45e-03	1.46	2.10e-01	0.02
1120	1.67e-01	1.15e-03	1.10	2.03e-01	0.05
6208	8.33e-02	4.98e-04	1.21	1.76e-01	0.20

Table 41 Degree-2 polygonal spline approximation of solution to (62) with exact solution (64) when $\eta = 10^{-10}$, $C_1 = 0.1$, $c_2 = c_1 + \varepsilon\pi^2/4$

# P	Mesh	E_{RMS}	Rate	∇E_{RMS}	Rate
40	6.67e-01	1.64e-03	0.00	2.82e-02	0.00
208	3.33e-01	2.61e-04	2.65	1.03e-02	1.45
1120	1.67e-01	3.86e-05	2.76	3.60e-03	1.52
6208	8.33e-02	5.68e-06	2.76	1.23e-03	1.55

Table 42 Degree-2 polygonal spline approximation of solution to (62) with exact solution (64) when $\eta = 10^{-10}$, $C_1 = 0.1$, $c_2 = c_1 + \varepsilon\pi^2/4$

# P	Mesh	E_{RMS}	Rate	∇E_{RMS}	Rate
40	6.67e-01	1.65e-03	0.00	2.62e-02	0.00
208	3.33e-01	2.48e-04	2.73	8.87e-03	1.56
1120	1.67e-01	3.80e-05	2.71	3.33e-03	1.42
6208	8.33e-02	5.65e-06	2.75	1.20e-03	1.47

Although this PDE does not technically fit our computational scheme due to the inclusion of first-order terms, we can still get a fairly good estimate of the true solution using degree-2 polygonal splines. Numerical results are shown in Table 40.

If we change the value of c_2 to $0.1 + \varepsilon\pi^2/4$, so that the solution is continuous, we retrieve the following results (without forcing continuity over the line $y = 0$). See Table 41.

Enforcing continuity over the line $y = 0$ leads to the results in Table 42.

From Tables 41 and 42, we can see that the computational results are very similar.

References

1. G. Awanou, M.-J. Lai, P. Wenston, The multivariate spline method for scattered data fitting and numerical solution of partial differential equations, in *Wavelets and Splines: Athens* (2006), pp. 24–74
2. L. Beirao da Veiga, F. Brezzi, A. Cangiani, G. Manzini, L. Marini, A. Russo, Basic principles of virtual element methods. Math. Models Methods Appl. Sci. **23** (2013)
3. L. Beirao da Veiga, K. Lipnikov, G. Manzini, Arbitrary-order nodal mimetic discretizations of elliptic problems on polygonal meshes. SIAM J. Numer. Anal. **49**, 1737–1760 (2011)
4. L. Beirao da Veiga, G. Manzini, A virtual element method with arbitrary regularity. IMA J. Numer. Anal. **34**, 759–781 (2014)
5. K. Bey, J. Oden, hp-version discontinuous galerkin methods for hyperbolic conservation laws. Comput. Methods Appl. Mech. Eng. **133**, 259–286 (1996)
6. D. Braess, *Finite Elements* (Cambridge University Press, Cambridge, 1997)
7. S. Brennet, L. Scott, *The Mathematical Theory of Finite Element Methods* (Springer, Berlin, 1994)
8. P. Ciarlet, *The Finite Element Method for Elliptic Problems* (North-Holland, 1978)
9. L. Evans, *Partial Differential Equations* (American Math. Society, 1998)
10. M. Floater, Generalized barycentric coordinates and applications. Acta Numerica **24**, 161–214 (2015)
11. M. Floater, A. Gillette, N. Sukumar, Gradient bounds for wachspress coordinates on polytopes. SIAM J. Numer. Anal. **52**, 515–532 (2014)
12. M. Floater, M.-J. Lai, Polygonal spline spaces and the numerical solution of the poisson equation. SIAM J. Numer. Anal. **54**, 797–824 (2016)
13. P. Grisvard, *Elliptic Problems in Nonsmooth Domains* (Pitman Advanced Pub. Program, 1985)
14. P. Houston, C. Schwab, E. Suli, Stabilized hp-finite element methods for first-order hyperbolic problems. SIAM J. Numer. Anal. **37**, 1618–1643 (2000)
15. P. Houston, C. Schwab, E. Suli, Discontinuous hp-finite element methods for advection-diffusion problems. SIAM J. Numer. Anal. **39**, 2133–2163 (2002)
16. M.-J. Lai , L. Schumaker, *Spline Functions Over Triangulations* (Cambridge University Press, Cambridge, 2007)
17. G. Manzini, A. Russo, N. Sukumar, New perspectives on polygonal and polyhedral finite element methods. Math. Models Methods Appl. Sci **24**, 1665–1699 (2014)
18. L. Mu, J. Wang, Y. Wang, X. Ye, A computational study of the weak galerkin method for second-order elliptic equations. Numer. Algorithms **63**, 753–777 (2013)
19. L. Mu, J. Wang, X. Ye, Weak galerkin finite element methods on polytopal meshes. Int. J. Numer. Anal. **12**, 31–53 (2015)
20. A. Rand, A. Gillette, C. Bajaj, Quadratic serendipity finite elements on polygons using generalized barycentric coordinates. Math. Comput. **83**, 2691–2716 (2014)
21. L. Schumaker, *Spline Functions: Computational Methods* (SIAM, 2015)
22. E. Stein, *Singular Integrals and Differentiability Properties of Functions* (Princeton University Press, 1970)